

First-principle calculations of the Berry curvature of Bloch states for charge and spin transport of electrons

This article has been downloaded from IOPscience. Please scroll down to see the full text article.

2012 J. Phys.: Condens. Matter 24 213202

(<http://iopscience.iop.org/0953-8984/24/21/213202>)

View [the table of contents for this issue](#), or go to the [journal homepage](#) for more

Download details:

IP Address: 160.45.66.65

The article was downloaded on 16/10/2012 at 13:16

Please note that [terms and conditions apply](#).

TOPICAL REVIEW

First-principle calculations of the Berry curvature of Bloch states for charge and spin transport of electrons

M Gradhand^{1,2}, D V Fedorov^{1,3}, F Pientka^{3,4}, P Zahn^{3,5}, I Mertig^{1,3} and B L Györfy²

¹ Max Planck Institute of Microstructure Physics, Weinberg 2, 06120 Halle, Germany

² H H Wills Physics Laboratory, University of Bristol, Bristol BS8 1TH, UK

³ Institute of Physics, Martin Luther University Halle-Wittenberg, 06099 Halle, Germany

⁴ Dahlem Center for Complex Quantum Systems and Fachbereich Physik, Freie Universität Berlin, 14195 Berlin, Germany

⁵ Institute of Ion Beam Physics and Materials Research, Helmholtz-Zentrum Dresden-Rossendorf e.V., PO Box 510119, 01314 Dresden, Germany

E-mail: m.gradhand@bristol.ac.uk

Received 15 February 2012, in final form 3 April 2012

Published 11 May 2012

Online at stacks.iop.org/JPhysCM/24/213202

Abstract

Recent progress in wave packet dynamics based on the insight of Berry pertaining to adiabatic evolution of quantum systems has led to the need for a new property of a Bloch state, the Berry curvature, to be calculated from first principles. We report here on the response to this challenge by the *ab initio* community during the past decade. First we give a tutorial introduction of the conceptual developments we mentioned above. Then we describe four methodologies which have been developed for first-principle calculations of the Berry curvature. Finally, to illustrate the significance of the new developments, we report some results of calculations of interesting physical properties such as the anomalous and spin Hall conductivity as well as the anomalous Nernst conductivity and discuss the influence of the Berry curvature on the de Haas–van Alphen oscillation.

(Some figures may appear in colour only in the online journal)

Contents

1. Introduction: semiclassical electronic transport in solids, wave packet dynamics, and the Berry curvature	2	2. First-principle calculations of the Berry curvature for Bloch electrons	8
1.1. New features of the Boltzmann equation	2	2.1. KKR method	8
1.2. Berry phase, connection and curvature of Bloch electrons	3	2.2. Tight-binding model	10
1.3. Abelian and non-Abelian curvatures	4	2.3. Wannier interpolation scheme	13
1.4. Symmetry, topology, codimension and the Dirac monopole	5	2.4. Kubo formula	15
1.5. The spin polarization gauge	6	3. Intrinsic contribution to the charge and spin conductivity in metals	17
		4. De Haas–van Alphen oscillation and the Berry phases	20
		5. Conclusion	21
		Acknowledgments	22
		References	22

1. Introduction: semiclassical electronic transport in solids, wave packet dynamics, and the Berry curvature

Some recent, remarkable advances in the semiclassical description of charge and spin transport by electrons in solids motivate a revival of interest in a detailed \mathbf{k} -point by \mathbf{k} -point study of their band structure. A good summary of the conceptual developments and the experiments they have stimulated has been given by Di Xiao *et al* [1]. Here we wish to review only the role and prospects of first-principle electronic structure calculations in this rapidly moving field.

1.1. New features of the Boltzmann equation

Classically, particle transport is considered to take place in phase space, whose points are labeled by the position vector \mathbf{r} and the momentum \mathbf{p} , and is described by the distribution function $f(\mathbf{r}, \mathbf{p}, t)$, which satisfies the Boltzmann equation. Electrons in solids fit into this framework if we view the particles as wave packets constructed from the Bloch waves, $\Psi_{n\mathbf{k}}(\mathbf{r}) = e^{i\mathbf{k}\cdot\mathbf{r}} u_n(\mathbf{r}, \mathbf{k})$, eigenfunctions of the unperturbed crystal Hamiltonian \hat{H}_0 with band index n and the dispersion relation $\mathcal{E}_{n\mathbf{k}}$. If such a wave packet is strongly centered at \mathbf{k}_c in the Brillouin zone, it predominantly includes Bloch states with quantum numbers \mathbf{k} close to \mathbf{k}_c and the particle can be said to have a momentum $\hbar\mathbf{k}_c$. Then, if we call its spatial center \mathbf{r}_c its position, the transport of electrons can be described by an ensemble of such quasiparticles. One of them is described by the distribution function $f_n(\mathbf{r}_c, \mathbf{k}_c, t)$. For simplicity, the band index n is dropped in the following for f , \mathbf{r}_c , and \mathbf{k}_c . As $f(\mathbf{r}_c, \mathbf{k}_c, t)$ evolves in phase space, the usual form of the Boltzmann equation, which preserves the total probability, is given by

$$\partial_t f + \dot{\mathbf{r}}_c \cdot \nabla_{\mathbf{r}_c} f + \dot{\mathbf{k}}_c \cdot \nabla_{\mathbf{k}_c} f = \left(\frac{\delta f}{\delta t} \right)_{\text{scatt}}. \quad (1)$$

Here the first term on the left hand side is the derivative with respect to the explicit time dependence of f , the next two terms account for the time dependence of \mathbf{r}_c and \mathbf{k}_c , and the term on the right-hand side describes the scattering of electron states, by defects and other perturbations, *in* and *out* of the considered phase space volume centered at \mathbf{r}_c and \mathbf{k}_c . The time evolution of $\mathbf{r}_c(t)$ and $\mathbf{k}_c(t)$ is given by semiclassical equations of motion, which in the presence of external electric \mathbf{E} and magnetic \mathbf{B} fields take conventionally the following form:

$$\dot{\mathbf{r}}_c = \left. \frac{1}{\hbar} \frac{\partial \mathcal{E}_{n\mathbf{k}}}{\partial \mathbf{k}} \right|_{\mathbf{k}=\mathbf{k}_c} = \mathbf{v}_n(\mathbf{k}_c), \quad (2)$$

$$\hbar \dot{\mathbf{k}}_c = -e\mathbf{E} - e\dot{\mathbf{r}}_c \times \mathbf{B}. \quad (3)$$

Here, the group velocity $\mathbf{v}_n(\mathbf{k}_c)$ involves the unperturbed band structure. In the presence of a constant electric $\mathbf{E} = (E_x, 0, 0)$ and magnetic $\mathbf{B} = (0, 0, B_z)$ field, the solution of the above equations yields the Hall resistivity $\rho_{xy} \propto B_z$. However, for a ferromagnet with magnetization $\mathbf{M} = (0, 0, M_z)$ the above theory cannot account for the experimentally

observed (additional) *anomalous* contribution $\rho_{xy} \propto M_z$. For a necessary correction of the theory, one needs to construct a wave packet [2]

$$W_{\mathbf{k}_c, \mathbf{r}_c}(\mathbf{r}, t) = \sum_{\mathbf{k}} a_{\mathbf{k}}(\mathbf{k}_c, t) \Psi_{n\mathbf{k}}(\mathbf{r}), \quad (4)$$

carefully taking into account the phase of the weighting function $a_{\mathbf{k}}(\mathbf{k}_c, t)$. Requiring the wave packet to be centered at $\mathbf{r}_c = \langle W_{\mathbf{k}_c, \mathbf{r}_c} | \mathbf{r} | W_{\mathbf{k}_c, \mathbf{r}_c} \rangle$ and considering zero order in the magnetic field only, it follows that $a_{\mathbf{k}}(\mathbf{k}_c, t) = |a_{\mathbf{k}}(\mathbf{k}_c, t)| e^{i(\mathbf{k}-\mathbf{k}_c) \cdot \mathbf{A}_n(\mathbf{k}_c) - i\mathbf{k} \cdot \mathbf{r}_c}$ [2], where

$$\mathbf{A}_n(\mathbf{k}_c) = i \int_{\text{u.c.}} d^3r u_n^*(\mathbf{r}, \mathbf{k}_c) \nabla_{\mathbf{k}} u_n(\mathbf{r}, \mathbf{k}_c) \quad (5)$$

is the *Berry connection*, as will be discussed in detail in section 1.2. Note that the integral is restricted to only one unit cell (uc). Now, using the wave packet of equation (4), one can construct the Lagrangian

$$L(t) = \langle W | i\hbar \partial_t - \hat{H} | W \rangle \quad (6)$$

and minimize the action functional $S[\mathbf{r}_c(t), \mathbf{k}_c(t)] = \int^t dt' L(t')$ with respect to arbitrary variations in $\mathbf{r}_c(t)$ and $\mathbf{k}_c(t)$. This maneuver replaces the quantum mechanical expectation values with respect to $W_{\mathbf{k}_c, \mathbf{r}_c}(\mathbf{r}, t)$ by the classical equations of motion for $\mathbf{r}_c(t)$ and $\mathbf{k}_c(t)$. From the Euler–Lagrange equations

$$\frac{d}{dt} \frac{\partial L}{\partial \dot{\mathbf{r}}_c} - \frac{\partial L}{\partial \mathbf{r}_c} = 0 \quad \text{and} \quad \frac{d}{dt} \frac{\partial L}{\partial \dot{\mathbf{k}}_c} - \frac{\partial L}{\partial \mathbf{k}_c} = 0, \quad (7)$$

one gets

$$\dot{\mathbf{r}}_c = \left. \frac{1}{\hbar} \frac{\partial \mathcal{E}_{n\mathbf{k}}}{\partial \mathbf{k}} \right|_{\mathbf{k}=\mathbf{k}_c} - \dot{\mathbf{k}}_c \times \boldsymbol{\Omega}_n(\mathbf{k}_c), \quad (8)$$

$$\hbar \dot{\mathbf{k}}_c = -e\mathbf{E} - e\dot{\mathbf{r}}_c \times \mathbf{B}. \quad (9)$$

Here $\boldsymbol{\Omega}_n(\mathbf{k}_c)$ is the so-called *Berry curvature*, defined as

$$\boldsymbol{\Omega}_n(\mathbf{k}_c) = \nabla_{\mathbf{k}} \times \mathbf{A}_n(\mathbf{k})|_{\mathbf{k}=\mathbf{k}_c}, \quad (10)$$

the main subject of this review. For simplicity, several further terms in equations (8) and (9) were neglected. These are fully discussed in [1, 2]. For the purpose of this review the above form is sufficient to highlight the occurrence of the Berry curvature in the equations of motion.

In comparison to equation (2), the new equation of motion for $\dot{\mathbf{r}}_c(t)$ given by equation (8) has an additional term proportional to the electric field called the *anomalous velocity*

$$\mathbf{v}_n^a(\mathbf{k}_c) = \frac{e}{\hbar} \mathbf{E} \times \boldsymbol{\Omega}_n(\mathbf{k}_c). \quad (11)$$

The presence of this velocity provides the anomalous contribution to the Hall current $j_y^H = j_y^{H, \uparrow} + j_y^{H, \downarrow}$, where the spin-resolved currents may be written as

$$j_y^{H, \uparrow} = -e \int_{BZ} \frac{d^3 k_c}{(2\pi)^3} j_{c\uparrow}^y(\mathbf{k}_c) f_{\uparrow}(\mathbf{k}_c) = \sigma_{yx}^{\uparrow}(M_z) E_x. \quad (12)$$

$$j_y^{H, \downarrow} = -e \int_{BZ} \frac{d^3 k_c}{(2\pi)^3} j_{c\downarrow}^y(\mathbf{k}_c) f_{\downarrow}(\mathbf{k}_c) = \sigma_{yx}^{\downarrow}(M_z) E_x. \quad (13)$$

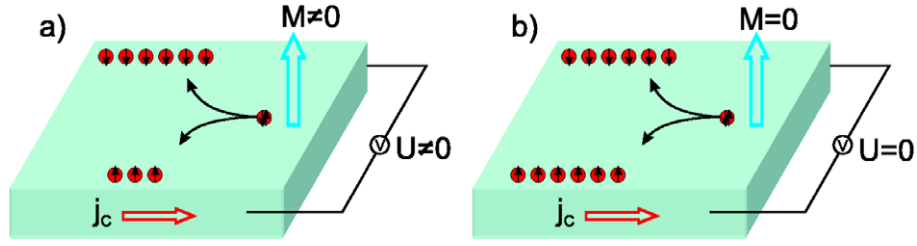


Figure 1. (a) The anomalous Hall effect and (b) the spin Hall effect.

In this notation $f_{\uparrow}(\mathbf{k}_c)$ and $f_{\downarrow}(\mathbf{k}_c)$ are the spin-resolved distribution functions which are solutions of equation (1). Here \mathbf{r}_c and t are dropped due to homogeneous and steady state conditions. In the limit of no scattering they reduce to the equilibrium distribution functions and only the intrinsic mechanism, governed by the anomalous velocity of equation (11), contributes to the Hall component. In general, $j_y^{H,\uparrow}$ and $j_y^{H,\downarrow}$ have opposite signs because of $\hat{\mathbf{r}}_{c\downarrow}(\mathbf{k}_c)$ and $\hat{\mathbf{r}}_{c\uparrow}(\mathbf{k}_c)$. However, the resulting charge current is nonvanishing (see figure 1(a)) due to the fact that the numbers of spin-up and spin-down electrons differ in ferromagnets with a finite magnetization $\mathbf{M} \neq 0$. In contrast to the anomalous Hall effect (AHE) in ferromagnets, the absence of the magnetization in normal metals leads to the presence of time inversion symmetry and, as a consequence, $j_y^{H,\uparrow} = -j_y^{H,\downarrow}$. This implies a vanishing charge current, i.e. Hall voltage, but the existence of a pure spin current as depicted in figure 1(b), which is known as the spin Hall effect (SHE).

1.2. Berry phase, connection and curvature of Bloch electrons

Here we introduce briefly the concept of such relatively novel quantities as the Berry phase, connection, and curvature which arise in the case of an adiabatic evolution of a system.

1.2.1. Adiabatic evolution and the Berry phase. Let us consider an eigenvalue problem of the following form:

$$\begin{aligned} \hat{H}(\mathbf{r}, \lambda_1, \lambda_2, \lambda_3) \Phi_n(\mathbf{r}; \lambda_1, \lambda_2, \lambda_3) \\ = \mathcal{E}_n(\lambda_1, \lambda_2, \lambda_3) \Phi_n(\mathbf{r}; \lambda_1, \lambda_2, \lambda_3), \end{aligned} \quad (14)$$

where \hat{H} is a differential operator, Φ_n and \mathcal{E}_n are the n th eigenfunction and eigenvalue, respectively, the vector \mathbf{r} is a variable, and $\lambda_1, \lambda_2, \lambda_3$ are parameters. A mathematical problem of general interest is the way such eigenfunctions change if the set $\boldsymbol{\lambda} = (\lambda_1, \lambda_2, \lambda_3)$ changes slowly with time. If it is assumed that the process is adiabatic, that is to say there is no transition from one to another state, then for a long time it was argued that a state $\Phi_n(\mathbf{r}, \boldsymbol{\lambda}, t)$ evolves in time as $\Phi_n(\mathbf{r}, \boldsymbol{\lambda}, t) = \Phi_n(\mathbf{r}, \boldsymbol{\lambda}) \exp(-\frac{i}{\hbar} \int_0^t dt' \mathcal{E}_n(\lambda_1(t'), \lambda_2(t'), \lambda_3(t')) + i\gamma_n(t))$, where the phase $\gamma_n(t)$ is meaningless as it can be gauged away. In 1984 Berry [3] discovered that, while this is true for an arbitrary open path in the parameter space, for a path that returns to the starting values $\lambda_1(0), \lambda_2(0)$, and $\lambda_3(0)$ the accumulated phase is gauge invariant and is therefore a meaningful and measurable

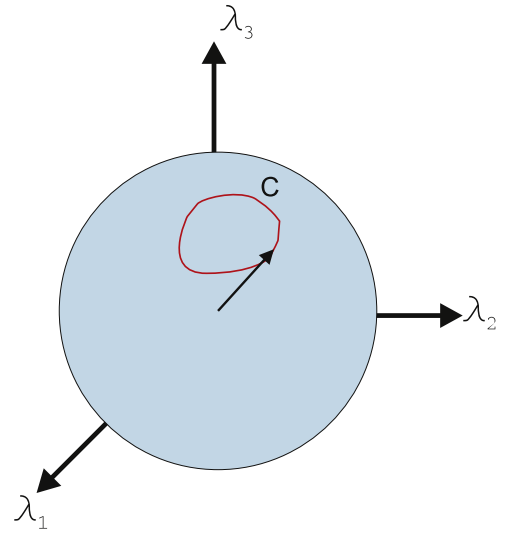


Figure 2. A closed path in the parameter space.

quantity. In particular, he showed that for a closed path, labeled C in figure 2, the phase γ_n , called the Berry phase today, can be described by a line integral as

$$\gamma_n = \oint_C d\boldsymbol{\lambda} \cdot \mathbf{A}_n(\boldsymbol{\lambda}), \quad (15)$$

where the connection $\mathbf{A}_n(\boldsymbol{\lambda})$ is given by

$$\mathbf{A}_n(\boldsymbol{\lambda}) = i \int d^3r \Phi_n^*(\mathbf{r}, \boldsymbol{\lambda}) \nabla_{\boldsymbol{\lambda}} \Phi_n(\mathbf{r}, \boldsymbol{\lambda}). \quad (16)$$

The surprise is that, although the connection is not gauge invariant, γ_n and even more interestingly the curvature

$$\boldsymbol{\Omega}_n(\boldsymbol{\lambda}) = \nabla_{\boldsymbol{\lambda}} \times \mathbf{A}_n(\boldsymbol{\lambda}) \quad (17)$$

are. As will be shown presently, these ideas are directly relevant for the dynamics of wave packets in the transport theory discussed above.

1.2.2. Berry connection and curvature for Bloch states. Somewhat surprisingly, the above discussion has a number of interesting things to say about the wave packets in the semiclassical approach for spin and charge transport of electrons in crystals. Its relevance becomes evident if we take the Schrödinger equation for the Bloch state

$$\left(-\frac{\hbar^2}{2m} \nabla_{\mathbf{r}}^2 + V(\mathbf{r}) \right) \Psi_{n\mathbf{k}}(\mathbf{r}) = \mathcal{E}_{n\mathbf{k}} \Psi_{n\mathbf{k}}(\mathbf{r}) \quad (18)$$

and rewrite it for the periodic part of the Bloch function

$$\left(-\frac{\hbar^2}{2m}(\nabla_{\mathbf{r}} + i\mathbf{k})^2 + V(\mathbf{r})\right)u_n(\mathbf{r}, \mathbf{k}) = \mathcal{E}_{n\mathbf{k}}u_n(\mathbf{r}, \mathbf{k}). \quad (19)$$

The point is that the differential equation for $\Psi_{n\mathbf{k}}(\mathbf{r})$, a simultaneous eigenfunction of the translation operator and the Hamiltonian, does not depend on the wave vector, since \mathbf{k} only labels the eigenvalues of the translation operator. However, in equation (19) \mathbf{k} appears as a parameter and hence the above discussion of the Berry phase, the corresponding connection, and curvature applies directly to the periodic part of the wave function $u_n(\mathbf{r}, \mathbf{k})$. In short, for each band n there is a connection associated with every \mathbf{k} given by

$$\mathbf{A}_n(\mathbf{k}) = i \int_{\text{uc}} d^3r u_n^*(\mathbf{r}, \mathbf{k}) \nabla_{\mathbf{k}} u_n(\mathbf{r}, \mathbf{k}). \quad (20)$$

Furthermore, the curvature

$$\begin{aligned} \Omega_n(\mathbf{k}) &= \nabla_{\mathbf{k}} \times \mathbf{A}_n(\mathbf{k}) \\ &= i \int_{\text{uc}} d^3r \nabla_{\mathbf{k}} u_n^*(\mathbf{r}, \mathbf{k}) \times \nabla_{\mathbf{k}} u_n(\mathbf{r}, \mathbf{k}) \end{aligned} \quad (21)$$

is the quantity that appears in the semiclassical equation of motion for the wave packet in equation (8). Thus, the curvature and the corresponding anomalous velocity in equations (11) associated with the band n are properties of $u_n(\mathbf{r}, \mathbf{k})$. To emphasize this point, we note that the Bloch functions $\Psi_{n\mathbf{k}}(\mathbf{r})$ are orthogonal to each other

$$\langle \Psi_{n\mathbf{k}} | \Psi_{n'\mathbf{k}'} \rangle = \int_{\text{crystal}} d^3r \Psi_{n\mathbf{k}}^*(\mathbf{r}) \Psi_{n'\mathbf{k}'}(\mathbf{r}) = \delta_{\mathbf{k}, \mathbf{k}'} \delta_{n, n'}, \quad (22)$$

and hence \mathbf{k} is not a parameter. In contrast, $u_n(\mathbf{r}, \mathbf{k})$ is orthogonal to $u_{n'}(\mathbf{r}, \mathbf{k})$ but not necessarily to $u_n(\mathbf{r}, \mathbf{k}')$, as this is an eigenfunction of a different Hamiltonian.

The observation that the above connection and curvature are properties of the periodic part of the Bloch function prompts a further comment. Note that for vanishing periodic potential the Bloch functions would reduce to plane waves. Constructing the wave packet from plane waves means $u_n(\mathbf{r}, \mathbf{k}) = 1$. Evidently, this means that $\Omega_n(\mathbf{k})$ and $\mathbf{A}_n(\mathbf{k})$ vanish, and this fact is consistent with the general notion that the connection and the curvature arise from including only one or in any case a finite number of bands in constructing the wave packet. The point is that the neglected bands are the ‘outside world’ referred to in the original article of Berry [3]. In contrast, the expansion in terms of plane waves does not neglect any bands since there is just one band. Thus, the physical origin of the connection and the curvature is due to the periodic crystal potential breaking up the full spectrum of the parabolic free particle dispersion relation into bands. They are usually separated by gaps, and we select states only from a limited number of such bands to represent the wave packet.

1.3. Abelian and non-Abelian curvatures

So far we have introduced the Berry connection and curvature for a nondegenerate band. In the case of degenerate bands the conventional adiabatic theorem fails. In the

semiclassical framework a correct treatment incorporates a wave packet constructed from the degenerate bands [4, 5]. As a consequence, the Berry curvature must be extended to a tensor definition in analogy to non-Abelian gauge theories. This extension is originally due to Wilczek and Zee [6].

Let us consider the eigenspace $\{|u_i(\mathbf{k})\rangle : i \in \Sigma\}$ of some N -fold degenerate eigenvalue. For Bloch states the elements of the non-Abelian Berry connection $\bar{\mathbf{A}}(\mathbf{k})$ read

$$\mathbf{A}_{ij}(\mathbf{k}) = i \langle u_i(\mathbf{k}) | \nabla_{\mathbf{k}} u_j(\mathbf{k}) \rangle \quad i, j \in \Sigma, \quad (23)$$

where $\Sigma = \{1, \dots, N\}$ contains all indices of the degenerate subspace. The definition of the curvature tensor $\bar{\Omega}(\mathbf{k})$ in a non-Abelian gauge theory has to be extended by substituting the curl with the covariant derivative as [5]

$$\begin{aligned} \bar{\Omega}(\mathbf{k}) &= \nabla_{\mathbf{k}} \times \bar{\mathbf{A}}(\mathbf{k}) - i \bar{\mathbf{A}}(\mathbf{k}) \times \bar{\mathbf{A}}(\mathbf{k}), \\ \Omega_{ij}(\mathbf{k}) &= i \left\langle \frac{\partial u_i(\mathbf{k})}{\partial \mathbf{k}} \middle| \times \middle| \frac{\partial u_j(\mathbf{k})}{\partial \mathbf{k}} \right\rangle \\ &\quad + i \sum_{l \in \Sigma} \left\langle u_i(\mathbf{k}) \middle| \frac{\partial u_l(\mathbf{k})}{\partial \mathbf{k}} \right\rangle \times \left\langle u_l(\mathbf{k}) \middle| \frac{\partial u_j(\mathbf{k})}{\partial \mathbf{k}} \right\rangle. \end{aligned} \quad (24)$$

The subspace of degenerate eigenstates is subject to a $U(N)$ gauge freedom and observables should be invariant with respect to a gauge transformation of the basis set

$$\left\{ \sum_i U_{ji}(\mathbf{k}) |u_i(\mathbf{k})\rangle : i \in \Sigma \right\} \quad \text{with } \bar{U}(\mathbf{k}) \in U(N). \quad (25)$$

Consequently, the Berry connection and curvature are transformed according to

$$\bar{\mathbf{A}}'(\mathbf{k}) = \bar{U}^\dagger(\mathbf{k}) \bar{\mathbf{A}}(\mathbf{k}) \bar{U}(\mathbf{k}) + i \bar{U}^\dagger(\mathbf{k}) \nabla_{\mathbf{k}} \bar{U}(\mathbf{k}), \quad (26)$$

$$\bar{\Omega}'(\mathbf{k}) = \bar{U}^\dagger(\mathbf{k}) \bar{\Omega}(\mathbf{k}) \bar{U}(\mathbf{k}). \quad (27)$$

The curvature is now a *covariant* tensor and thus not directly observable. However, there are gauge invariant quantities that may be derived from it. From gauge theories it is known that the connection and the curvature must lie in the tangent space of the gauge group $U(N)$, i.e., the Lie algebra $\mathfrak{u}(N)$. The above definition of the Lie algebra differs by an unimportant factor of i from the mathematical convention.

The most prominent example of a non-Abelian Berry curvature appears in materials with time-reversal (T) and inversion (I) symmetry. For each \mathbf{k} point there exist two orthogonal states $|\Psi_{n\uparrow\mathbf{k}}\rangle$ and $|\Psi_{n\downarrow\mathbf{k}}\rangle = \text{TI}|\Psi_{n\uparrow\mathbf{k}}\rangle$ with the same energy, the Kramers doublet. In general, a choice for $|\Psi_{n\uparrow\mathbf{k}}\rangle$ determines the second basis state $|\Psi_{n\downarrow\mathbf{k}}\rangle$ only up to a phase. However, the symmetry transformation fixes the phase relationship between the two basis states. This reduces the gauge freedom to $SU(2)$ and, consequently, the Berry connection will be an $\mathfrak{su}(2)$ matrix, which means the trace of the 2×2 matrix vanishes. This is verified easily

$$\begin{aligned} \langle u_{n\downarrow}(\mathbf{k}) | \nabla_{\mathbf{k}} u_{n\downarrow}(\mathbf{k}) \rangle &= \langle \text{TI} u_{n\uparrow}(\mathbf{k}) | \nabla_{\mathbf{k}} \text{TI} u_{n\uparrow}(\mathbf{k}) \rangle \\ &= \langle \text{TI} u_{n\uparrow}(\mathbf{k}) | \text{TI} \nabla_{\mathbf{k}} u_{n\uparrow}(\mathbf{k}) \rangle \\ &= -\langle u_{n\uparrow}(\mathbf{k}) | \nabla_{\mathbf{k}} u_{n\uparrow}(\mathbf{k}) \rangle. \end{aligned} \quad (28)$$

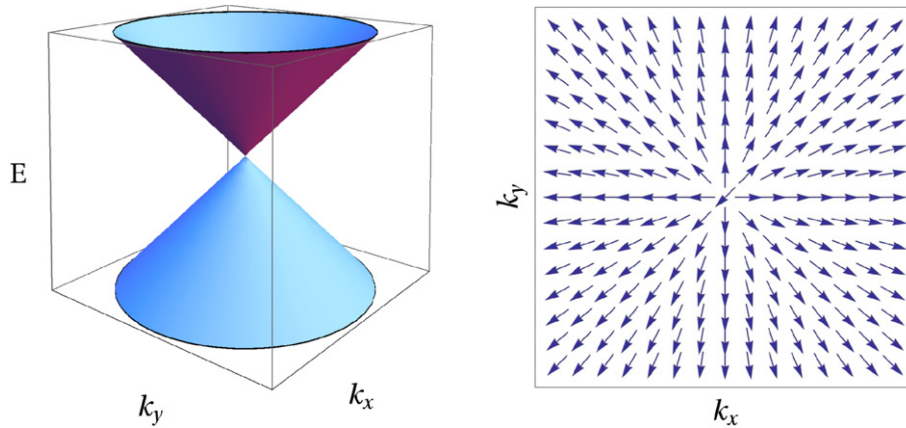


Figure 3. Left: conical intersection of energy surfaces. Right: direction of the monopole field $\Omega_+(\mathbf{k})$.

For the Kramers doublet the Berry curvature must always be an $\mathfrak{su}(2)$ matrix even in the case of a $u(2)$ connection because a gauge transformation induces a unitary transformation of the curvature which does not alter the trace. Indeed, $\text{Tr} \Omega_{n\uparrow\uparrow}(\mathbf{k}) = -\Omega_{n\uparrow\uparrow}(\mathbf{k}) = \Omega_{n\downarrow\downarrow}(\mathbf{k})$, which proves that the trace is equal to zero. Therefore, in contrast to the spinless case, discussed in the next section, the Berry curvature may be nontrivial even in nonmagnetic materials with inversion symmetry.

Despite the Berry curvature being gauge covariant, we may derive several observables from it. As we have seen, the trace of the Berry curvature is gauge invariant. In the multiband formulation of the semiclassical theory, the expectation value of the curvature matrix with respect to the spinor amplitudes enters the equations of motion [4, 5]. In the context of the spin Hall effect one is interested in $\text{Tr}(\bar{S}^\alpha \bar{\Omega}^\beta)$, where \bar{S}^α is the α th component of the vector-valued $\mathfrak{su}(2)$ spin matrix (cf section 2.4.2).

1.4. Symmetry, topology, codimension and the Dirac monopole

It is expedient to exploit symmetries of the Hamiltonian for the evaluation of the Berry curvature. From equations (20) and (21) we may easily determine the behavior of $\Omega_n(\mathbf{k})$ under symmetry operations. In crystals with a center of inversion, the corresponding symmetry operation leaves $\mathcal{E}_{n\mathbf{k}}$ invariant while \mathbf{r} , $\dot{\mathbf{r}}$, \mathbf{k} , and $\dot{\mathbf{k}}$ change sign, and hence $\Omega_n(\mathbf{k}) = \Omega_n(-\mathbf{k})$. On the other hand, when time-reversal symmetry is present, $\mathcal{E}_{n\mathbf{k}}$, \mathbf{r} , and $\dot{\mathbf{k}}$ remain unchanged while $\dot{\mathbf{r}}$ and \mathbf{k} are inverted, which leads to an antisymmetric Berry curvature $\Omega_n(\mathbf{k}) = -\Omega_n(-\mathbf{k})$. Thus, if time-reversal and inversion symmetry are present simultaneously the Berry curvature vanishes identically [7]. This is true for spinless particles only. Taking into account spin, we have to acknowledge the presence of a twofold degeneracy of all bands throughout the Brillouin zone [8, 9], the Kramers doublet, discussed in the previous section.

As was mentioned already in section 1.2.2, the Berry curvature of a band arises due to the attempt of a single-band description; e.g., in the semiclassical theory it keeps the

information about the influence of other adjacent bands. If a band is well separated from all other bands by an energy scale large compared to one set by the time scale of the adiabatic evolution, the influence of the other bands is negligible. In contrast, degeneracies of energy bands deserve special attention, since the conventional adiabatic theorem fails in this case. Special attention has been paid to point-like degeneracies, where the intersection of two energy bands is shaped like a double cone or a diabolical point. These degeneracies are called diabolical points [10]. A typical one, studied within a tight-binding model in [11], is shown in figure 3.

In general, a Hermitian Hamiltonian $\hat{H}(\mathbf{k})$ with three parameters k_x, k_y, k_z has degeneracies (band crossings) at points \mathbf{k}^* . Taking \mathbf{k}^* as the origin and assuming that $\hat{H}(\mathbf{k})$ depends linearly on the \mathbf{k} measured from \mathbf{k}^* , a generic example for two bands crossing can be constructed as follows.

At $\mathbf{k} = \mathbf{k}^*$ there are two orthogonal states $|a\rangle$ and $|b\rangle$ whose energies are the same, $\mathcal{E}_a = \mathcal{E}_b = 0$, which we take to be the energy zero. In the vicinity of the point \mathbf{k}^* we can express the eigenstates in terms of the two states

$$|u_n(\mathbf{k})\rangle = c_{an}(\mathbf{k}) |a\rangle + c_{bn}(\mathbf{k}) |b\rangle \quad (29)$$

where $n = \{+, -\}$ and the coefficients $c_{an}(\mathbf{k})$ and $c_{bn}(\mathbf{k})$ are determined by the eigenvalue problem

$$\hat{H}(\mathbf{k}) |u_n(\mathbf{k})\rangle = \mathcal{E}_{n\mathbf{k}} |u_n(\mathbf{k})\rangle. \quad (30)$$

Using the expansion of equation (29), little is lost in generality by taking $\hat{H}(\mathbf{k})$ in the representation of the two states $|a\rangle$ and $|b\rangle$ to be of the form [3]

$$H(\mathbf{k}) = \begin{pmatrix} k_z & k_x - ik_y \\ k_x + ik_y & -k_z \end{pmatrix}, \quad (31)$$

and hence the eigenvalue equation can be written as

$$\begin{pmatrix} k_z & k_x - ik_y \\ k_x + ik_y & -k_z \end{pmatrix} \begin{pmatrix} c_{an}(\mathbf{k}) \\ c_{bn}(\mathbf{k}) \end{pmatrix} = \mathcal{E}_{n\mathbf{k}} \begin{pmatrix} c_{an}(\mathbf{k}) \\ c_{bn}(\mathbf{k}) \end{pmatrix}. \quad (32)$$

The solution of this eigenvalue problem is

$$\mathcal{E}_{\pm\mathbf{k}} = \pm \sqrt{k_z^2 + k_x^2 + k_y^2} = \pm |\mathbf{k}| = \pm k \quad (33)$$

and the two eigenvectors are

$$u_+(\mathbf{k}) \equiv \begin{pmatrix} c_{a+}(\mathbf{k}) \\ c_{b+}(\mathbf{k}) \end{pmatrix} = \begin{pmatrix} \sqrt{\frac{k+k_z}{2k}} e^{-i\frac{\delta_+}{2}} \\ \sqrt{\frac{k-k_z}{2k}} e^{+i\frac{\delta_+}{2}} \end{pmatrix} \quad (34)$$

$$\delta_+ = \tan^{-1}\left(\frac{k_y}{k_x}\right) \quad (35)$$

$$u_-(\mathbf{k}) \equiv \begin{pmatrix} c_{a-}(\mathbf{k}) \\ c_{b-}(\mathbf{k}) \end{pmatrix} = \begin{pmatrix} \sqrt{\frac{k-k_z}{2k}} e^{-i\frac{\delta_-}{2}} \\ -\sqrt{\frac{k+k_z}{2k}} e^{+i\frac{\delta_-}{2}} \end{pmatrix} \quad (36)$$

$$\delta_- = \tan^{-1}\left(\frac{k_y}{k_x}\right) \quad (37)$$

where we used the shortcut $u_{\pm}(\mathbf{k})$ for the two component eigenvectors representing the expansion coefficients of $|u_n(\mathbf{k})\rangle$. Clearly, $\delta_+ = \delta_- \equiv \delta$ holds.

Calculating the connection

$$\mathbf{A}_+(\mathbf{k}) = i u_+^\dagger(\mathbf{k}) \nabla_{\mathbf{k}} u_+(\mathbf{k}) \quad (38)$$

and the curvature as

$$\Omega_+(\mathbf{k}) = -\text{Im} \frac{u_+^\dagger(\mathbf{k}) \nabla_{\mathbf{k}} \hat{H}(\mathbf{k}) u_-(\mathbf{k}) \times u_-^\dagger(\mathbf{k}) \nabla_{\mathbf{k}} \hat{H}(\mathbf{k}) u_+(\mathbf{k})}{(\mathcal{E}_+\mathbf{k} - \mathcal{E}_-\mathbf{k})^2} \quad (39)$$

one finds

$$\Omega_{\pm}(\mathbf{k}) = \mp \frac{1}{2} \frac{\mathbf{k}}{k^3}. \quad (40)$$

This is precisely the form of the magnetic field due to a Dirac monopole, if \mathbf{k} is replaced by the real space vector \mathbf{r} , with the magnetic charges $\mp \frac{1}{2}$ [3] (see figure 3, right). Diabolical points always have this charge, while nonlinear intersections may have higher charges [12]. In general, the monopole charge is a topological invariant and quantized to integer multiples of $1/2$. This is a consequence of the quantization of the Dirac monopole [13].

In more general language, the Berry curvature flux through a closed two-dimensional manifold ∂M is the first Chern number C_n of that manifold and thus an integer. Since the (Abelian) curvature is defined as the curl of the connection, it must be divergence free except for the monopoles. We can then exploit Gauss's theorem

$$\begin{aligned} C_n &= \frac{1}{2\pi} \int_{\partial M} d\sigma \Omega_n(\mathbf{k}) \mathbf{n}(\mathbf{k}) \\ &= \frac{1}{2\pi} \int_M d^3k \nabla_{\mathbf{k}} \cdot \Omega_n = m, \quad m \in \mathbb{N}. \end{aligned} \quad (41)$$

Here \mathbf{n} is the normal vector of the surface element. If we assume that each monopole contributes a Chern number of ± 1 the above equation implies for the Berry curvature $\nabla_{\mathbf{k}} \cdot \Omega(\mathbf{k}) = 4\pi \sum_j g_j \delta(\mathbf{k} - \mathbf{k}_j^*)$, where $g_j = \pm 1/2$. The solution of this differential equation yields the source term of the Berry

curvature

$$\Omega(\mathbf{k}) = \sum_j g_j \frac{\mathbf{k} - \mathbf{k}_j^*}{|\mathbf{k} - \mathbf{k}_j^*|^3} + \nabla_{\mathbf{k}} \times \mathbf{A}(\mathbf{k}), \quad (42)$$

which proves that there are monopoles with a charge quantized to $1/2$ times an integer.

The mathematical interpretation of the Berry curvature in terms of the theory of fiber bundles and Chern classes and the connection to the theory of the quantum Hall effect, where the Chern number appears as the Thouless–Kohmoto–Nightingale–den Nijs (TKNN) integer [14] was first noticed by Simon [15].

However, monopoles are interesting not only in a mathematical sense but also for actual physical quantities such as the anomalous Hall conductivity. On the one hand, singularities of the Berry curvature near the Fermi surface greatly influence the numerical stability of calculations of physical properties. On the other hand, as Haldane [16] has pointed out, the Chern number and thus the anomalous Hall conductivity can be changed by creation and annihilation of Berry curvature monopoles.

To identify monopoles in a parameter space, one is interested in degeneracies that do not occur on account of any symmetry and have thus been called accidental. For a single Hamiltonian without symmetries the occurrence of degeneracies in the discrete spectrum is infinitely unlikely. For Hamiltonians that depend on a set of parameters one can ask how many parameters are needed in order to encounter a twofold degenerate eigenvalue. This number is called the codimension. According to a theorem by von Neumann and Wigner [17], for a generic Hamiltonian the answer is three. In other words, degeneracies are points in a three-dimensional parameter space like the Brillouin zone. For this reason accidental degeneracies are diabolical points.

If the Hamiltonian is *real*, which is equivalent to being invariant with respect to time reversal, the number of parameters we have to vary reduces to two [18]. However, we have seen that in the case of nonmagnetic crystals with inversion symmetry each band is twofold degenerate. This degeneracy arises due to a symmetry and is not accidental. The theorem of von Neumann and Wigner does not apply. As a consequence, *accidental* degeneracies of two different bands would have to be fourfold. In this case the codimension is five and the occurrence of an accidental degeneracy is infinitely unlikely in the Brillouin zone. This is the reason why we only observe avoided crossings for nonmagnetic crystals with inversion symmetry. All accidental crossings are lifted by spin–orbit coupling. In order to encounter accidental twofold degeneracies of codimension three, we would, thus, need to consider a nonmagnetic band structure without inversion symmetry of the lattice.

1.5. The spin polarization gauge

As has been discussed in the previous sections, in spinless crystals with time-reversal and inversion symmetry the Berry curvature vanishes at every \mathbf{k} point [7]. If spin degrees of freedom are taken into account the band structure is twofold

degenerate throughout the Brillouin zone due to Kramers degeneracy plus inversion symmetry, and consequently the Berry curvature is represented by an element of the Lie algebra $\mathfrak{su}(2)$. In contrast to the Abelian case, this matrix is gauge covariant and hence not observable. However, at least two gauge invariant quantities can be derived from the Berry curvature matrix. First of all, the trace is gauge invariant but equal to zero at all \mathbf{k} points in the considered situation of nonmagnetic, inversion symmetric systems. In addition, the determinant of the covariant matrix is gauge invariant, which might be used to visualize the non-Abelian Berry curvature. Since this quantity is gauge invariant it should be observable. In general, a correct non-Abelian theory for physical observables must be derived to make use of the full Berry curvature matrix. Nevertheless a simplified single-band picture, where just the diagonal elements of the Berry curvature are used, might be helpful if an approximate theory is applied. Then a certain gauge has to be chosen. For example, in the case of the spin Hall conductivity it was shown [19] that the diagonal element of the Berry curvature in a certain gauge leads to good approximation to the results from full quantum mechanical approaches. With respect to first-principle calculations the necessary choice of gauge was discussed in the literature [20–22]. The idea of this section is to discuss two possible gauges and to compare their implications for matrix quantities such as the spin polarization and the Berry curvature.

One natural choice of a gauge, let us call it gauge I, is to ensure that the spin polarization of one Kramers state $|\Psi_{\uparrow\mathbf{k}}\rangle$ is parallel to the z direction *and* positive [22], that is

$$\begin{aligned} \langle \Psi_{\uparrow\mathbf{k}} | \sigma_x | \Psi_{\uparrow\mathbf{k}} \rangle &= 0, \\ \langle \Psi_{\uparrow\mathbf{k}} | \sigma_y | \Psi_{\uparrow\mathbf{k}} \rangle &= 0, \\ \langle \Psi_{\uparrow\mathbf{k}} | \sigma_z | \Psi_{\uparrow\mathbf{k}} \rangle &> 0. \end{aligned} \quad (43)$$

This means that for the second Kramers state $|\Psi_{\downarrow\mathbf{k}}\rangle$

$$\langle \Psi_{\downarrow\mathbf{k}} | \sigma_z | \Psi_{\downarrow\mathbf{k}} \rangle = -\langle \Psi_{\uparrow\mathbf{k}} | \sigma_z | \Psi_{\uparrow\mathbf{k}} \rangle < 0. \quad (44)$$

More generally, we will discuss the spin polarization as an $\mathfrak{su}(2)$ matrix $(\tilde{\mathbf{S}}_n(\mathbf{k}))_{ij} = \langle \Psi_{i\mathbf{k}} | \boldsymbol{\sigma} | \Psi_{j\mathbf{k}} \rangle$ with $i, j = \uparrow, \downarrow$, as it appears in the context of the spin Hall effect. Conditions (43) then imply that the diagonal elements are aligned along the z direction in this gauge. The positiveness of the first diagonal element is essential, since in this way we can distinguish the two degenerate states. However, this fails when the spin polarization goes to zero within this gauge.

As a result of the theorem by von Neumann and Wigner [17] discussed in section 1.4, we do not expect accidental degeneracies in nonmagnetic materials. They are lifted by spin–orbit coupling. When two bands get close at some point in the Brillouin zone they ‘repel’ each other depending on the strength of spin–orbit coupling. The lifting of accidental degeneracies by spin–orbit coupling, at a certain point Q in momentum space, is illustrated in figure 4 with and without spin–orbit interaction, displayed in red and black, respectively. Similar to real crossings in the magnetic case, there are peaks of the Berry curvature at these points, since the two degenerate bands under consideration are significantly

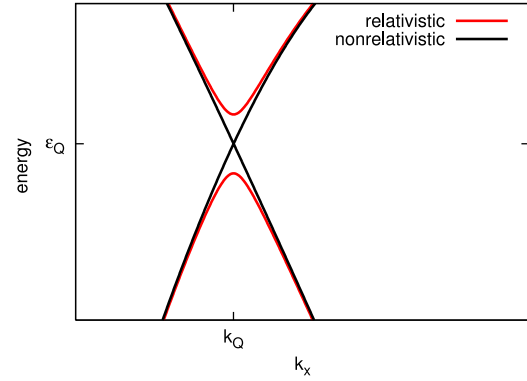


Figure 4. Band structure with (red) and without (black) spin–orbit coupling around point Q obtained within tight-binding calculations [11]. The fourfold accidental degeneracy of the nonmagnetic band structure is lifted.

influenced by the neighboring bands. However, in contrast to the magnetic case, the curvature remains finite.

When introducing gauge I, we remarked that it is necessary to enforce a positive sign of $\langle \Psi_{\uparrow\mathbf{k}} | \sigma_z | \Psi_{\uparrow\mathbf{k}} \rangle$ in addition to the alignment of the spin polarization along the z axis. By doing so one can distinguish the two degenerate Kramers states $|\Psi_{\uparrow\mathbf{k}}\rangle$ and $|\Psi_{\downarrow\mathbf{k}}\rangle$ according to their spin polarization. This criterion becomes useless once there is a point where the spin polarization vanishes in the chosen gauge. This is exactly the case when the avoided crossing originates from an accidental degeneracy lifted by spin–orbit coupling.

This situation is illustrated in figure 5, where the spin polarization for both Kramers states of the lower doublet is shown. The spin polarization becomes zero at the avoided crossing. In fact, the picture suggests that the spin polarizations of both states change sign, which means that by enforcing gauge I we have changed from the first to the second Kramers state while crossing point Q . Indeed, this is verified by the graph of the first diagonal element of the Berry curvature in this gauge presented in figure 5. Exactly at the point where the spin polarization vanishes, the Berry curvature changes sign, jumping from one degenerate state of the band to the other. This jump is unsatisfactory, since it does not allow us to follow the Berry curvature consistently throughout the BZ without adjustment by hand. A way out is provided by a different gauge.

This new gauge (let us call it gauge II) describes the nonmagnetic crystal as the limit of vanishing exchange splitting in a magnetic crystal. The task is then to find the unitary transformation that diagonalizes the perturbation operator H_{xc} in the degenerate subspace of the Kramers doublet. This amounts to the condition

$$\langle \Psi_{\uparrow\mathbf{k}} | \mathcal{H}_{xc} | \Psi_{\downarrow\mathbf{k}} \rangle \propto \langle \Psi_{\uparrow\mathbf{k}} | \sigma_z | \Psi_{\downarrow\mathbf{k}} \rangle = 0. \quad (45)$$

The above equation accounts for the two free parameters we have to fix. Furthermore, we choose the sign as

$$\langle \Psi_{\uparrow\mathbf{k}} | \sigma_z | \Psi_{\uparrow\mathbf{k}} \rangle > 0. \quad (46)$$

In gauge II the diagonal elements of the nonmagnetic spin expectation value of each state represent the analytical

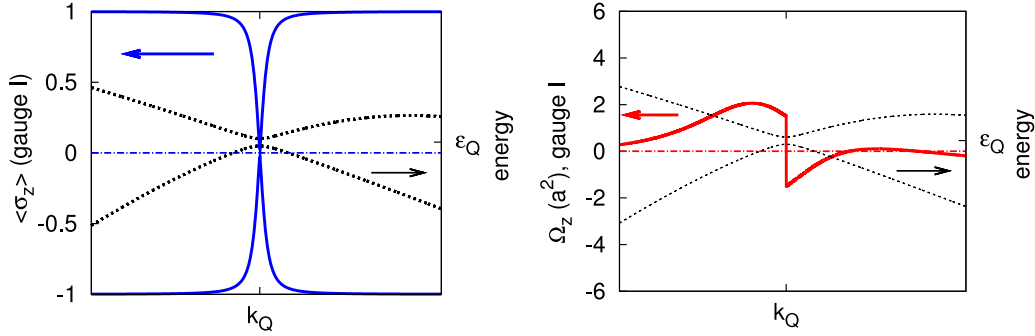


Figure 5. The band structure of two bands (black dotted lines) near an avoided crossing at point Q in momentum space (see figure 4). Left: both diagonal elements of the $\mathfrak{su}(2)$ spin polarization (blue full lines) of the Kramers doublet of the lower band in gauge I. Right: the first diagonal element of the $\mathfrak{su}(2)$ Berry curvature $\Omega_{\uparrow\uparrow,z}$ (red full lines) of the same band jumps in gauge I. a denotes the lattice parameter. See also [23].

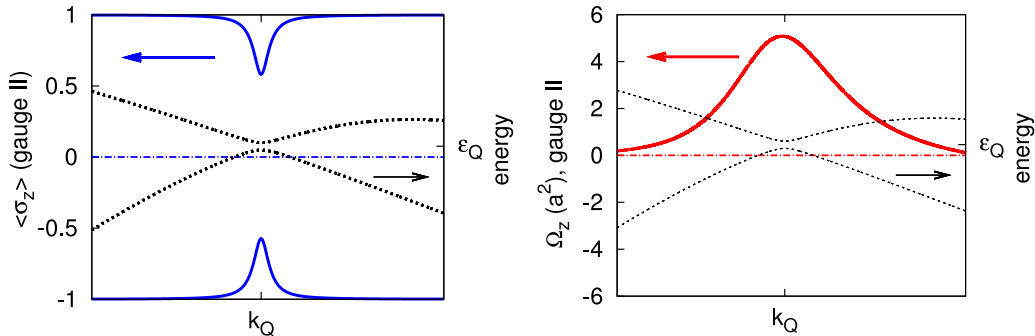


Figure 6. The band structure of two bands (black dotted lines) near an avoided crossing at point Q in momentum space (see figure 4). Left: both diagonal elements of the nonmagnetic spin polarization (blue) of the lower doublet in gauge II. Right: the first diagonal element of the $\mathfrak{su}(2)$ Berry curvature—see figure 5 (red)—remains continuous in gauge II. See also [23].

continuation of the magnetic spin polarizations with vanishing exchange splitting.

In figure 6 the same avoided crossing as in figure 5 is shown while gauge II has been imposed. The spin polarization now remains finite and the Berry curvature is continuous, thus we have resolved the ambiguity. This result is clearly an advantage of gauge II in comparison to gauge I. Furthermore, it can be shown that gauge II maximizes the diagonal element of the σ_z operator [23] with respect to all possible gauges. This implies that, for a proper discussion of spin hot spots, the vanishing of the spin expectation value, gauge II has to be chosen. A comparative study of the implications of the gauge choice in actual first-principle calculation will be presented elsewhere [23].

2. First-principle calculations of the Berry curvature for Bloch electrons

2.1. KKR method

2.1.1. Berry connection. In this section we describe the most recent of four methods developed for calculating the Berry curvature within first-principle computational schemes. This approach [19] is based on the screened version of the venerable Korringa–Kohn–Rostoker (KKR) method [24, 25] and is motivated by the fact that in the multiple

scattering theory the wave vector \mathbf{k} enters the problem only through the structure constants $G_{QQ'}^s(\mathcal{E}; \mathbf{k})$. These depend on the geometrical arrangement of the scatterers but not on the scattering potentials at the lattice sites. Hence the sort of \mathbf{k} derivative that occur in the definition of the connection in equation (20) should involve only the derivative $\nabla_{\mathbf{k}} G_{QQ'}^s(\mathcal{E}; \mathbf{k})$, easy to calculate within the screened KKR method. In what follows we demonstrate that such an expectation can indeed be realized, and an efficient algorithm is readily constructed which takes full advantage of these features.

As is clear from equations (20) and (21), the connection $\mathbf{A}_n(\mathbf{k})$ and the curvature $\Omega_n(\mathbf{k})$ are the properties of the periodic component $u_n(\mathbf{r}, \mathbf{k})$ of the Bloch state $\Psi_{n\mathbf{k}}(\mathbf{r})$. However, as in most band theory methods, in the KKR one calculates the Bloch wave. Thus, to facilitate the calculation of $\mathbf{A}_n(\mathbf{k})$ and $\Omega_n(\mathbf{k})$ from $\Psi_{n\mathbf{k}}(\mathbf{r})$, one must recast the problem. A useful way to proceed with it is to rewrite

$$\begin{aligned} \mathbf{A}_n(\mathbf{k}) &= i \int_{\text{uc}} d^3r u_n^\dagger(\mathbf{r}, \mathbf{k}) \nabla_{\mathbf{k}} u_n(\mathbf{r}, \mathbf{k}) \\ &= i \int_{\text{uc}} d^3r \Psi_{n\mathbf{k}}^*(\mathbf{r}) \nabla_{\mathbf{k}} \Psi_{n\mathbf{k}}(\mathbf{r}) \\ &\quad + \int_{\text{uc}} d^3r \Psi_{n\mathbf{k}}^*(\mathbf{r}) \mathbf{r} \Psi_{n\mathbf{k}}(\mathbf{r}), \end{aligned} \quad (47)$$

where the integrals are performed over the unit cell.

Since the most interesting physical consequences of the Berry curvature occur in spin-orbit coupled systems, the theory is developed in terms of a fully relativistic multiple scattering theory based on the Dirac equation. In short, the four component Dirac Bloch wave [26] is expanded around the sites within the unit cell in terms of the local scattering solutions $\Phi_Q(\mathcal{E}; \mathbf{r})$ of the radial Dirac equation as [19]

$$\Psi_{n\mathbf{k}}(\mathbf{r}) = \sum_Q C_{n,Q}(\mathbf{k}) \Phi_Q(\mathcal{E}; \mathbf{r}), \quad (48)$$

where Q comprises site and spin-angular momentum indices. In such a representation the expansion coefficients $C_{n,Q}(\mathbf{k})$ are solutions of the eigenvalue problem

$$\begin{aligned} \bar{M}(\mathcal{E}; \mathbf{k}) \bar{C}_n(\mathbf{k}) &= \lambda_n(\mathcal{E}; \mathbf{k}) \bar{C}_n(\mathbf{k}) \\ \text{with } \bar{C}_n(\mathbf{k}) &= \{C_{n,Q}(\mathbf{k})\} \end{aligned} \quad (49)$$

for the KKR matrix [19]

$$M_{QQ'}(\mathcal{E}; \mathbf{k}) = G_{QQ'}^s(\mathcal{E}; \mathbf{k}) \Delta t_{Q'}^s(\mathcal{E}) - \delta_{QQ'}, \quad (50)$$

where $G_{QQ'}^s(\mathcal{E}; \mathbf{k})$ are the relativistic screened structure constants, $\Delta t_{Q'}^s(\mathcal{E})$ is the corresponding t matrix of the reference system with respect to the system under consideration [24] and the eigenvalues $\lambda_n(\mathcal{E}, \mathbf{k})$ vanish for $\mathcal{E} = \mathcal{E}_{n\mathbf{k}}$.

Note that the eigenvalue problem equation (49) depends parametrically on \mathbf{k} . Therefore, one can formally deploy the original arguments of Berry [3] to derive an expression for the curvature associated with this problem. Namely, one finds (here for the sake of simplicity we assume the matrix \bar{M} to be Hermitian) [3, 19]

$$\Omega_n^{\text{KKR}}(\mathbf{k}) = -\text{Im} \left\{ \sum_{m \neq n} \frac{\bar{C}_n^\dagger \nabla_{\mathbf{k}} \bar{M} \bar{C}_m \times \bar{C}_m^\dagger \nabla_{\mathbf{k}} \bar{M} \bar{C}_n}{(\lambda_n - \lambda_m)^2} \right\}. \quad (51)$$

The rhs has to be evaluated at an energy $\mathcal{E} = \mathcal{E}_{n\mathbf{k}}$, so λ_n is equal to zero. Evidently, this curvature is a property of the KKR matrix $\bar{M}(\mathcal{E}; \mathbf{k})$. What is important about this result is the fact that the \mathbf{k} derivative operates only on $\bar{M}(\mathcal{E}; \mathbf{k})$ and therefore it can be expressed simply by

$$\partial \bar{G}^s(\mathcal{E}; \mathbf{k}) / \partial \mathbf{k} = i \sum_{\mathbf{R}} \mathbf{R} e^{i\mathbf{k}\cdot\mathbf{R}} \bar{G}^s(\mathcal{E}; \mathbf{R}), \quad (52)$$

which can be easily evaluated since the screened real space structure constants $\bar{G}^s(\mathcal{E}; \mathbf{R})$ are short ranged. While this is reassuringly consistent with the expectation at the beginning of this section, it is not the whole story. The curvature of the KKR matrix is not that of the Hamiltonian

$$\hat{H}_{\mathbf{k}}(\mathbf{r}) = e^{-i\mathbf{k}\cdot\mathbf{r}} \hat{H}(\mathbf{r}) e^{i\mathbf{k}\cdot\mathbf{r}}, \quad (53)$$

whose eigenfunctions are the periodic components $u_n(\mathbf{r}, \mathbf{k})$. In fact, when we evaluate equation (47) we find

$$\mathbf{A}_n(\mathbf{k}) = \mathbf{A}_n^k(\mathbf{k}) + \mathbf{A}_n^r(\mathbf{k}) = \mathbf{A}_n^{\text{KKR}}(\mathbf{k}) + \mathbf{A}_n^v(\mathbf{k}) + \mathbf{A}_n^r(\mathbf{k}). \quad (54)$$

Here we have the KKR part

$$\mathbf{A}_n^{\text{KKR}}(\mathbf{k}) = i \bar{C}_n^\dagger \nabla_{\mathbf{k}} \bar{C}_n = -\text{Im} \{ \bar{C}_n^\dagger \nabla_{\mathbf{k}} \bar{C}_n \}, \quad (55)$$

the velocity part

$$\mathbf{A}_n^v(\mathbf{k}) = i \hbar \mathbf{v}_n \bar{C}_n^\dagger \bar{\Delta} \bar{C}_n = -\hbar \mathbf{v}_n \text{Im} \{ \bar{C}_n^\dagger \bar{\Delta} \bar{C}_n \}, \quad (56)$$

with

$$(\bar{\Delta})_{QQ'}(\mathcal{E}) = \delta_{QQ'} \int_{\text{uc}} d^3r \Phi_Q^\dagger(\mathcal{E}; \mathbf{r}) \frac{\partial \Phi_{Q'}(\mathcal{E}; \mathbf{r})}{\partial \mathcal{E}}, \quad (57)$$

and the dipole part

$$\mathbf{A}_n^r(\mathbf{k}) = \bar{C}_n^\dagger(\mathbf{k}) \bar{\mathbf{r}} \bar{C}_n(\mathbf{k}), \quad (58)$$

with the matrix elements of the position operator

$$(\bar{\mathbf{r}})_{QQ'}(\mathcal{E}) = \int_{\text{uc}} d^3r \Phi_Q^\dagger(\mathcal{E}; \mathbf{r}) \mathbf{r} \Phi_{Q'}(\mathcal{E}; \mathbf{r}). \quad (59)$$

As will be shown, the contribution from the first term of the rhs of equation (54) provides the curvature associated with the KKR matrix in equation (51), while the velocity term $\mathbf{A}_n^v(\mathbf{k})$ and dipole term $\mathbf{A}_n^r(\mathbf{k})$ lead to small corrections.

2.1.2. Abelian Berry curvature. Starting from the Berry connection introduced above it is straightforward to extend the method to the Berry curvature expressions. For the Abelian case the Berry curvature is given by three contributions

$$\begin{aligned} \Omega_n(\mathbf{k}) &= \nabla_{\mathbf{k}} \times \mathbf{A}_n(\mathbf{k}) = \Omega_n^k(\mathbf{k}) + \Omega_n^r(\mathbf{k}) \\ &= \Omega_n^{\text{KKR}}(\mathbf{k}) + \Omega_n^v(\mathbf{k}) + \Omega_n^r(\mathbf{k}), \end{aligned} \quad (60)$$

stemming from the analog terms in equation (54). Here, the KKR part, which is shown to be the dominant contribution [19], takes the simple form

$$\Omega_n^{\text{KKR}}(\mathbf{k}) = i \nabla_{\mathbf{k}} \bar{C}_n^\dagger \times \nabla_{\mathbf{k}} \bar{C}_n = -\text{Im} \{ \nabla_{\mathbf{k}} \bar{C}_n^\dagger \times \nabla_{\mathbf{k}} \bar{C}_n \}, \quad (61)$$

where just the expansion coefficients are involved. Now, an important step is to shift the \mathbf{k} derivative towards the \mathbf{k} -dependent KKR matrix. Actually, because of the chosen KKR-basis set in equation (48), one has to deal with a non-Hermitian KKR matrix. However, in order to simplify the further discussion and to have a clear insight into the presented approach, here the matrix \bar{M} is assumed to be Hermitian. Then, introducing a complete set of eigenvectors of the KKR matrix leads to equation (51), which is quite similar to that obtained in the original paper of Berry [3]. The difference is just that the \mathbf{k} -dependent Hamiltonian is replaced by the \mathbf{k} -dependent KKR matrix of finite dimension. As was already discussed, the partial \mathbf{k} derivative of the KKR matrix can be calculated analytically within the screened KKR method. In a similar way the velocity and the dipole terms, $\Omega_n^v(\mathbf{k})$ and $\Omega_n^r(\mathbf{k})$, can be treated. Both contributions are typically one order of magnitude smaller than the KKR part [19]. Moreover, the velocity part of the Berry curvature is always strictly perpendicular to the group velocity. This fact is a technically very important feature, since for a Fermi surface integral over the Berry curvature this contribution vanishes.

2.1.3. Non-Abelian Berry curvature. For a treatment of the non-Abelian Berry curvature not only the conventional connection has to be taken into account, but also the

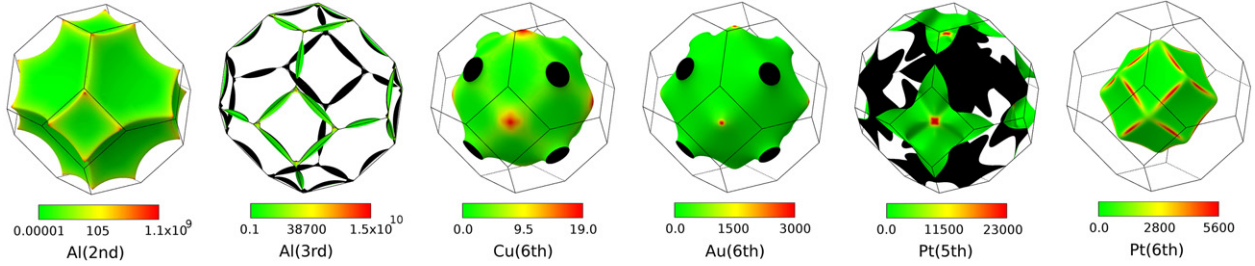


Figure 7. The absolute value (in a.u.) of the determinant of the non-Abelian Berry curvature $|\text{Det}[\Omega_{ij}(\mathbf{k})]|$ for the Fermi surface of several metals. From left to right, Al (second and third bands), Cu (sixth band), Au (sixth band) and Pt (fifth and sixth bands). For Al we used a logarithmic scale to enhance the important regions.

commutator, which is provided by the requirement of the gauge invariant theory, has to be considered [5]. As a consequence, the Berry curvature is defined as

$$\Omega_{ij}(\mathbf{k}) = i\langle \nabla_{\mathbf{k}} u_i(\mathbf{k}) | \times | \nabla_{\mathbf{k}} u_j(\mathbf{k}) \rangle - i \sum_{l \in \Sigma} \langle \nabla_{\mathbf{k}} u_i(\mathbf{k}) | u_l(\mathbf{k}) \rangle \times \langle u_l(\mathbf{k}) | \nabla_{\mathbf{k}} u_j(\mathbf{k}) \rangle. \quad (62)$$

Here, as has been discussed in section 1.3, Σ contains all indices of the degenerate subspace. Rewriting it in terms of the Bloch states yields

$$\begin{aligned} \Omega_{ij}(\mathbf{k}) &= i\langle \nabla_{\mathbf{k}} \Psi_{i\mathbf{k}} | \times | \nabla_{\mathbf{k}} \Psi_{j\mathbf{k}} \rangle + \langle \nabla_{\mathbf{k}} \Psi_{i\mathbf{k}} \times \mathbf{r} | \Psi_{j\mathbf{k}} \rangle \\ &\quad - \langle \Psi_{i\mathbf{k}} | \mathbf{r} \times \nabla_{\mathbf{k}} \Psi_{j\mathbf{k}} \rangle \\ &\quad - \sum_{l \in \Sigma} \{ i\langle \nabla_{\mathbf{k}} \Psi_{i\mathbf{k}} | \Psi_{l\mathbf{k}} \rangle \times \langle \Psi_{l\mathbf{k}} | \nabla_{\mathbf{k}} \Psi_{j\mathbf{k}} \rangle \\ &\quad - \langle \Psi_{i\mathbf{k}} | \mathbf{r} | \Psi_{l\mathbf{k}} \rangle \times \langle \Psi_{l\mathbf{k}} | \nabla_{\mathbf{k}} \Psi_{j\mathbf{k}} \rangle \\ &\quad + \langle \nabla_{\mathbf{k}} \Psi_{i\mathbf{k}} | \Psi_{l\mathbf{k}} \rangle \times \langle \Psi_{l\mathbf{k}} | \mathbf{r} | \Psi_{j\mathbf{k}} \rangle \\ &\quad + i\langle \Psi_{i\mathbf{k}} | \mathbf{r} | \Psi_{l\mathbf{k}} \rangle \times \langle \Psi_{l\mathbf{k}} | \mathbf{r} | \Psi_{j\mathbf{k}} \rangle \}, \end{aligned} \quad (63)$$

and a similar decomposition into the KKR, velocity and dipole parts

$$\Omega_{ij}(\mathbf{k}) = \Omega_{ij}^{\text{KKR}}(\mathbf{k}) + \Omega_{ij}^v(\mathbf{k}) + \Omega_{ij}^r(\mathbf{k}) \quad (64)$$

can be performed.

In figure 7 the absolute value of the determinant $|\text{Det}[\Omega_{ij}^z(\mathbf{k})]|$ of the non-Abelian (vector-valued matrix) Berry curvature over the Fermi surface of several metals is shown. This quantity is gauge invariant as has been discussed in section 1.5 and is convenient to visualize for a Kramers degenerate band. Near degeneracies at the Fermi level lead to enhanced Berry curvatures, as can be seen for Al and Pt. Interestingly, the values for Al are much larger than in Au, even though it is much lighter than the noble metal. The origins are the mentioned near degeneracies of Al at the Fermi level, which have been discussed in the literature [22, 20]. Furthermore, the energy resolved Berry curvature (here $S(\mathcal{E})$ is the constant energy \mathcal{E} surface in the \mathbf{k} space)

$$\Omega^z(\mathcal{E}) = \sum_n \frac{1}{\hbar} \int_{S(\mathcal{E})} \frac{d^2k}{|v^n(\mathbf{k})|} \Omega_n^{z,\uparrow}(\mathbf{k}) \quad (65)$$

is shown in figure 8. Here $\Omega_n^{z,\uparrow}(\mathbf{k}) = \Omega_{n,11}^z(\mathbf{k})$ denotes the first diagonal element of the Berry curvature in gauge II as discussed in section 1.5 with the positive spin polarization

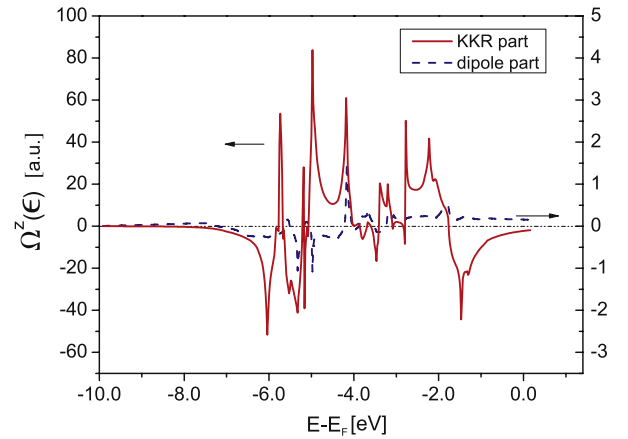


Figure 8. The energy resolved Berry curvature $\Omega^z(\mathcal{E})$ for Au divided into the parts $\Omega^{\text{KKR}}(\mathcal{E})$ and $\Omega^r(\mathcal{E})$ according to equation (64). The part $\Omega^v(\mathcal{E})$ is negligibly small and not shown. Reproduced with permission from [19]. Copyright 2011 American Physical Society.

$\langle \Psi_{\uparrow\mathbf{k}} | \beta \Sigma_z | \Psi_{\uparrow\mathbf{k}} \rangle > 0$ of the considered state. It proves that the KKR part of equation (64) is the dominant contribution to the Berry curvature. Clearly visible is the quite spiky structure of the curvature as a function of the energy. As discussed in the literature, this makes the integration of the Berry curvature computationally demanding, requiring a large number of \mathbf{k} and energy points.

2.2. Tight-binding model

The tight-binding (TB) model provides a convenient framework for studying the geometric quantities in band theory. We will briefly introduce the tight-binding method with spin-orbit coupling and exchange interaction. The usefulness of this model is then illustrated by discussing interesting features of the Berry curvature of a simple band structure, studied in [11].

2.2.1. Definition of the TB Hamiltonian. The tight-binding model assumes that the electronic wave function at each lattice site is well localized around the position of the atom. For this purpose one assumes the crystal potential to consist of a sum of spherically symmetric, somewhat strongly attractive potentials located at the core positions. The idea is to treat the

overlap matrix elements as a perturbation and consequently expand the wave function in a basis of atomic orbitals $\{\phi_\alpha(\mathbf{r} - \mathbf{R})\}$. The ansatz

$$\Psi_{n\mathbf{k}}(\mathbf{r}) = \frac{1}{\sqrt{N_R}} \sum_{\mathbf{R}} e^{i\mathbf{k}\mathbf{R}} \sum_{\alpha} C_{n\alpha}(\mathbf{k}) \phi_\alpha(\mathbf{r} - \mathbf{R}) \quad (66)$$

ensures that $\Psi_{n\mathbf{k}}$ fulfils the Bloch theorem with the lattice vectors \mathbf{R} . The simplest case involves neglecting the overlap matrix elements of the wave function

$$\langle \phi_\beta(\mathbf{r} - \mathbf{R}) | \phi_\alpha(\mathbf{r} - \mathbf{R}') \rangle \sim \delta_{\alpha,\beta} \delta_{\mathbf{R},\mathbf{R}'}. \quad (67)$$

The normalized eigenfunctions in this on-site approximation are subject to the eigenvalue problem $\langle \Psi_{n\mathbf{k}} | H | \Psi_{n\mathbf{k}} \rangle = \mathcal{E}_{n\mathbf{k}}$. The solution to this problem in the tight-binding formulation of equation (66) requires the diagonalization of the tight-binding matrix

$$H_{\alpha\beta}(\mathbf{k}) = \sum_{\mathbf{R},\mathbf{R}'} e^{i\mathbf{k}(\mathbf{R}-\mathbf{R}')} \langle \phi_\alpha(\mathbf{r} - \mathbf{R}') | H | \phi_\beta(\mathbf{r} - \mathbf{R}) \rangle. \quad (68)$$

Then the coefficients $C_{n\alpha}(\mathbf{k})$ are obtained as the components of the eigenvector of this matrix and thus the eigenstates necessary for the evaluation of the Berry curvature are easily accessible.

The matrix elements in equation (68) can be parametrized by the method of Slater and Koster [27]. In order to observe a nontrivial Berry curvature we need to take into account spin degrees of freedom. This doubles the number of bands compared to the spinless case. Within the scope of the tight-binding model the spin-orbit interaction is treated as a perturbation

$$V_{\text{SOC}} = \frac{\hbar}{4m^2c^2} (\nabla_{\mathbf{r}} V(\mathbf{r}) \times \mathbf{p}) \mathbf{S} = \frac{2\lambda}{\hbar^2} \mathbf{L} \mathbf{S} \quad (69)$$

to the Hamiltonian. Here a spherically symmetric potential is assumed and the parameter λ is considered to be small with respect to the on-site and hopping energies in equation (68). The matrix elements of this operator have been listed elsewhere for basis states of p, d and f symmetry [28] in an on-site approximation, although the formalism presented here does not require this approximation.

Furthermore, one can use this model to describe a ferromagnetic material by incorporating an exchange interaction term. The simplest formulation originates from the mean-field theory. Without taking into account any temperature dependence, a constant exchange field is assumed and the z axis is chosen as the quantization direction

$$H_{xc} = -\mathbf{V}_{xc} \boldsymbol{\sigma} = -V_{xc} \sigma_z, \quad (70)$$

where V_{xc} is a positive real number.

2.2.2. Berry curvature. As in the case of the KKR method discussed in section 2, solving the eigenproblem of the tight-binding matrix gives the Bloch wave $|\Psi_{n\mathbf{k}}\rangle$ instead of the periodic function $|u_n(\mathbf{k})\rangle$. Hence, one also needs to consider the two parts, $\Omega^k(\mathbf{k})$ and $\Omega^r(\mathbf{k})$, of the Berry curvature introduced by equation (60). Exploiting the on-site approximation of equation (67) and the normalization

condition for the coefficients, one gets the first term for the Abelian case in a well known form

$$\begin{aligned} \Omega_n^k(\mathbf{k}) &= i \langle \nabla_{\mathbf{k}} \Psi_{n\mathbf{k}} | \times | \nabla_{\mathbf{k}} \Psi_{n\mathbf{k}} \rangle_{\text{uc}} = i \nabla_{\mathbf{k}} \bar{C}_n^\dagger(\mathbf{k}) \times \nabla_{\mathbf{k}} \bar{C}_n(\mathbf{k}) \\ &= -\text{Im} \sum_{m \neq n} \frac{\bar{C}_n^\dagger(\mathbf{k}) \nabla_{\mathbf{k}} \bar{H}(\mathbf{k}) \bar{C}_m(\mathbf{k}) \times \bar{C}_m^\dagger(\mathbf{k}) \nabla_{\mathbf{k}} \bar{H}(\mathbf{k}) \bar{C}_n(\mathbf{k})}{(\mathcal{E}_{n\mathbf{k}} - \mathcal{E}_{m\mathbf{k}})^2}. \end{aligned} \quad (71)$$

The second, the dipole term, is given by

$$\begin{aligned} \Omega_n^r(\mathbf{k}) &= \nabla_{\mathbf{k}} \times \langle \Psi_{n\mathbf{k}} | \mathbf{r} | \Psi_{n\mathbf{k}} \rangle_{\text{cell}} = \nabla_{\mathbf{k}} \times (\bar{C}_n^\dagger(\mathbf{k}) \bar{\mathbf{r}} \bar{C}_n(\mathbf{k})) \\ &= \sum_{m \neq n} 2 \text{Re} \left[\frac{\bar{C}_n^\dagger(\mathbf{k}) \nabla_{\mathbf{k}} \bar{H}(\mathbf{k}) \bar{C}_m(\mathbf{k})}{\mathcal{E}_{n\mathbf{k}} - \mathcal{E}_{m\mathbf{k}}} \right. \\ &\quad \left. \times (\bar{C}_m^\dagger(\mathbf{k}) \bar{\mathbf{r}} \bar{C}_n(\mathbf{k})) \right], \end{aligned} \quad (72)$$

where we have introduced the vector-valued matrix $\bar{\mathbf{r}}$ with the components $\mathbf{r}_{\alpha\beta} = \langle \phi_\beta(\mathbf{r}) | \mathbf{r} | \phi_\alpha(\mathbf{r}) \rangle$. Similar to the screened KKR method, the \mathbf{k} derivative of $\bar{H}(\mathbf{k})$ in the equations above may be performed analytically and no numerical derivative is needed.

In the case of degenerate bands, the non-Abelian Berry curvature $\Omega_{ij}(\mathbf{k}) = \Omega_{ij}^k(\mathbf{k}) + \Omega_{ij}^r(\mathbf{k})$ is expressed in the following terms (according to section 1.3, Σ contains all indices of the degenerate subspace):

$$\Omega_{ij}^k(\mathbf{k}) = i \sum_{m \notin \Sigma} \frac{\bar{C}_i^\dagger(\mathbf{k}) \nabla_{\mathbf{k}} \bar{H}(\mathbf{k}) \bar{C}_m(\mathbf{k}) \times \bar{C}_m^\dagger(\mathbf{k}) \nabla_{\mathbf{k}} \bar{H}(\mathbf{k}) \bar{C}_j(\mathbf{k})}{(\mathcal{E}_{i\mathbf{k}} - \mathcal{E}_{m\mathbf{k}})(\mathcal{E}_{j\mathbf{k}} - \mathcal{E}_{m\mathbf{k}})}, \quad (73)$$

$$\begin{aligned} \Omega_{ij}^r(\mathbf{k}) &= \sum_{m \notin \Sigma} \left[-(\bar{C}_i^\dagger(\mathbf{k}) \bar{\mathbf{r}} \bar{C}_m(\mathbf{k})) \times \frac{\bar{C}_m^\dagger(\mathbf{k}) \nabla_{\mathbf{k}} \bar{H}(\mathbf{k}) \bar{C}_j(\mathbf{k})}{\mathcal{E}_{j\mathbf{k}} - \mathcal{E}_{m\mathbf{k}}} \right. \\ &\quad \left. + \frac{\bar{C}_i^\dagger(\mathbf{k}) \nabla_{\mathbf{k}} \bar{H}(\mathbf{k}) \bar{C}_m(\mathbf{k})}{\mathcal{E}_{i\mathbf{k}} - \mathcal{E}_{m\mathbf{k}}} \times (\bar{C}_m^\dagger(\mathbf{k}) \bar{\mathbf{r}} \bar{C}_j(\mathbf{k})) \right] \\ &\quad - i \sum_{l \in \Sigma} (\bar{C}_i^\dagger(\mathbf{k}) \bar{\mathbf{r}} \bar{C}_l(\mathbf{k})) \times (\bar{C}_l^\dagger(\mathbf{k}) \bar{\mathbf{r}} \bar{C}_j(\mathbf{k})). \end{aligned} \quad (74)$$

Here only the last term is not a direct generalization of the Abelian Berry curvature. Again it is possible to circumvent the numerical derivative by a summation over all states that do not belong to the degenerate subspace. The last term does not involve any derivative, therefore the sum runs only over the degenerate bands.

2.2.3. Diabolical points. To illustrate the behavior of the Berry curvature near degeneracies, we present calculations of a simple band structure using the tight-binding method. We consider a ferromagnetic simple cubic crystal with eight bands including one band with s symmetry and three bands with p symmetry for each spin direction. Due to the exchange interaction there is no time-reversal symmetry and the codimension of degeneracies is three.

Regions of the parameter space with a higher symmetry (e.g. high-symmetry lines in the Brillouin zone) are more likely to support accidental degeneracies because the

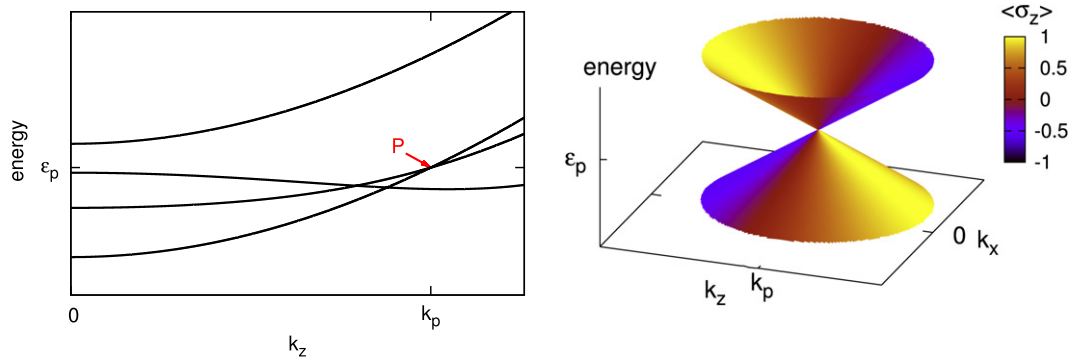


Figure 9. Left: the crossing of some p bands of a ferromagnetic simple cubic band structure near the center of the Brillouin zone. Right: conical intersection of energy surfaces near point P. The z axis represents the energy dispersion of two intersecting bands over an arbitrary plane in \mathbf{k} space through the diabolical point. The color scale denotes the spin polarization corresponding to each band.

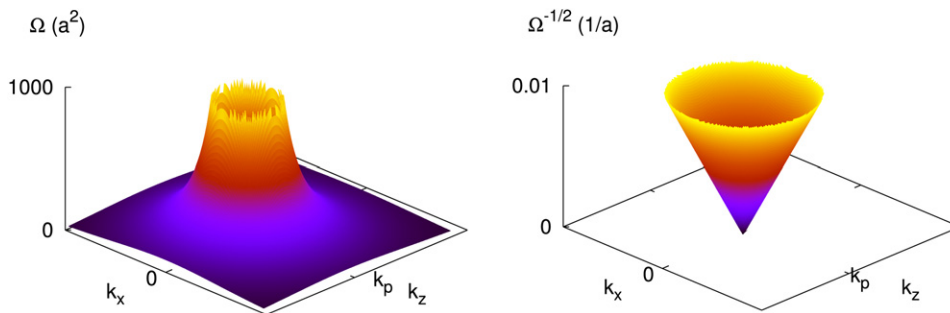


Figure 10. Left: absolute value of the Berry curvature $|\Omega|$ plotted over a plane in \mathbf{k} space through the degeneracy point P. Right: inverse square root of the absolute value, i.e. $1/\sqrt{|\Omega|}$.

symmetry possibly reduces the codimension only in this region. Level crossings on a high-symmetry line in the Brillouin zone do not necessarily occur on account of symmetry as long as the bands are not degenerate at points nearby which have the same symmetry.

As an example, in figure 9 a few bands of the band structure near the Γ point along a high-symmetry line are plotted. There occur three crossings between different bands. On the right-hand side, the energy dispersion in a plane through the degeneracy marked by P is displayed in order to show the cone shape of the intersection. The color scale represents the spin polarization $\langle \Psi | \sigma_z | \Psi \rangle$ of the corresponding band. Within one band the spin polarization rapidly changes in the vicinity of the degeneracy. At the degeneracy itself it jumps due to the cusp of the corresponding band. However, when passing the intersection along a straight line in \mathbf{k} space and jumping from the lower to the upper band apparently the spin polarization does not change at all. This is a clear indication that the character of the two bands is exchanged at the intersection.

The behavior of the spin polarization near the diabolical point illustrates how observables are influenced by other bands nearby. The Berry curvature can be viewed as a measure of this coupling, which becomes evident from equations (71) and (72), where a sum over all other bands is performed weighted by the inverse energy difference. Hence, the Berry curvature of a single Bloch band generally arises due to the restriction to this band and it becomes large when other

bands are close. As we have seen before, a degeneracy produces a singularity of the Berry curvature and the adiabatic single-band approximation fails.

In our case, the origin of the Berry curvature is the spin-orbit coupling. Since degenerate or almost degenerate points in the band structure produce large spin mixing of the involved bands, a peak in the Berry curvature can also be understood from this point of view.

As discussed in section 1.4, we would expect the curvature around the degeneracy to obey the $1/|\mathbf{k} - \mathbf{k}^*|^2$ law of a Coulomb field. The asymptotic behavior becomes evident when plotting $1/\sqrt{|\Omega|}$ in a plane in which the degeneracy is located (see figure 10 with $\mathbf{k}^* = (0, 0, k_p)$). We observe an absolute value function $|\mathbf{k} - \mathbf{k}^*|$, which proves that the Berry curvature really has the form of the monopole field strength given by equation (40).

Besides the absolute value we can also examine the direction of the Berry curvature vector. In figure 11, we recognize the characteristic monopole field. In the lower band the monopole is a source, in the upper band a drain, of the Berry curvature. This has been expected because a monopole in one band has to be matched by a monopole of opposite charge in the other band involved in the degeneracy.

In general, we may assign a ‘charge’ g to the monopole as in equation (42). This charge is quantized to be either integer or half integer. In order to determine the charge numerically one could perform a fit of the numerical data with the monopole field strength. However, there is no reason to

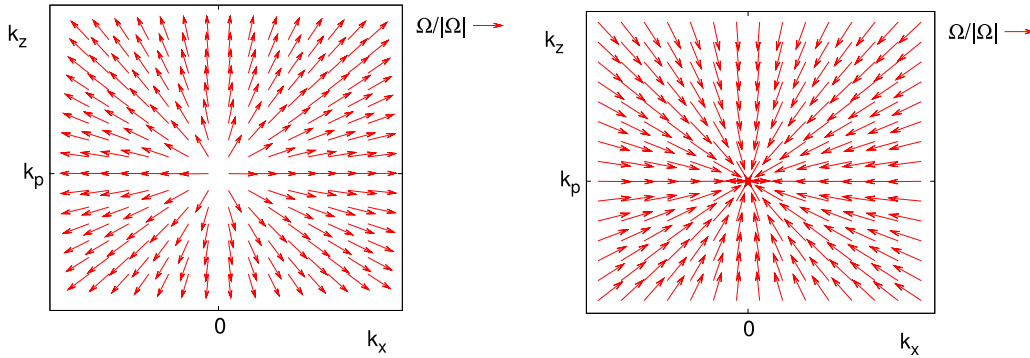


Figure 11. Normalized Berry curvature vector around P (compare figure 9, right panel).

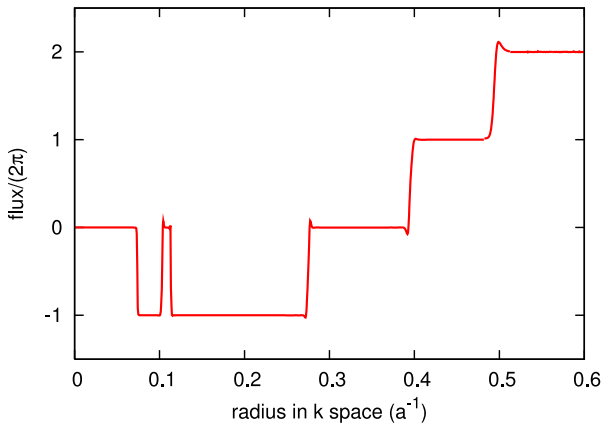


Figure 12. The value of the integral equation (75) over a spherical surface for the upper band is plotted against the radius of the sphere.

believe that all directions in \mathbf{k} space must be equivalent. Some distortion in a certain direction might result in ellipsoidal isosurfaces of $|\Omega|$ instead of spherical ones. A different approach, independent from the coordinate system, exploits equation (41)

$$\int_V d^3k \nabla_{\mathbf{k}} \cdot \Omega_n(\mathbf{k}) = \int_{\partial V} d\mathbf{s} \mathbf{n} \cdot \Omega_n(\mathbf{k}) = 2\pi m \quad m \in \mathbb{Z}, \tag{75}$$

where the vector \mathbf{n} is normal on the bounding surface ∂V of some arbitrary volume V . Performing the numerical surface integration causes no problem since the Berry curvature is analytical on the surface, unlike the case at the degeneracy. So as to validate this formula, the Berry curvature flux through a sphere of radius $|\mathbf{k} - \mathbf{k}_0|$ centered at a generic point \mathbf{k}_0 in the Brillouin zone near P (see figure 9) is evaluated. This flux divided by 2π as a function of the sphere's radius is plotted in figure 12.

The integral is observed to be quantized to integer multiples of 2π . When increasing the radius of the sphere the surface crosses various diabolical points. Each time this happens the flux jumps by $\pm 2\pi$ depending on whether the charge of the Berry curvature monopole is positive or negative. According to equation (75), this confirms that the charges of the monopoles created by the point-like degeneracies are $g = \pm 1/2$. Altogether there are six jumps,

which means there are six diabolical points in the vicinity of the point P (see figure 9). Two of the monopoles in the upper band have a negative, the other four a positive, charge of $1/2$. A generic point such as the center of the integration sphere is chosen to avoid crossing more than one diabolical point at a time. The deviations from a perfect step function are due to the discretization of the integral, which increases the error when the surface crosses a monopole. The step functions also verify the statement that monopoles are the only possible sources of the Berry curvature.

Haldane [16] describes the dynamics of these degeneracies with respect to the variation of some control parameter, including the creation of a pair of diabolical points and their recombination after relative displacement of a reciprocal lattice vector. In the considered case an obvious choice for the control parameters would be λ or V_{xc} , regulating the strength of spin-orbit coupling or exchange splitting, respectively.

Thus, the tight-binding code provides an excellent tool for an investigation of the effects connected with the accidental degeneracy of bands (see for instance, [16]) since one may scan through a whole range of parameters without consuming many computational resources and still obtain qualitatively reliable results.

2.3. Wannier interpolation scheme

The first method developed specifically for calculating the Berry curvature of Bloch electrons using the full machinery of the density functional theory (DFT) was based on the Wannier interpolation code of Marzari *et al* [29]. As in the case of the KKR method presented in section 2.1, the essence of this approach by Wang *et al* [21] is that it avoids taking the derivative of the periodic part of the Bloch function $u_n(\mathbf{r}, \mathbf{k})$ with respect to \mathbf{k} numerically by finite differences. A second almost equally important feature is that it offers various opportunities to interpolate between different \mathbf{k} points in the Brillouin zone and hence reduces the number of points at which full *ab initio* calculations need to be performed.

Note that the formulas, naturally arising in wave packet dynamics, for the Berry connection and curvature, given by equations (20) and (21), involve the real space integrals over a unit cell only. Extending them to cover all space by using the

Wannier functions defined as

$$|\mathbf{R}n\rangle = \frac{V_{uc}}{(2\pi)^3} \int_{BZ} d^3k e^{-i\mathbf{k}\cdot\mathbf{R}} |\Psi_{n\mathbf{k}}\rangle, \quad (76)$$

the Bloch theorem and some care with the algebra, one finds the following remarkably simple results [21, 30]:

$$\begin{aligned} \mathbf{A}_n(\mathbf{k}) &= \sum_{\mathbf{R}} \langle 0n | \mathbf{r} | \mathbf{R}n \rangle e^{i\mathbf{k}\cdot\mathbf{R}} \quad \text{and} \\ \Omega_n(\mathbf{k}) &= i \sum_{\mathbf{R}} \langle 0n | \mathbf{R} \times \mathbf{r} | \mathbf{R}n \rangle e^{i\mathbf{k}\cdot\mathbf{R}}. \end{aligned} \quad (77)$$

The matrix elements with respect to the Wannier states, as usual, involve integrals over all space. These formulas turn up and play a central role in the method of Wang *et al* [21] and make the Wannier interpolation approach look different from that based on the KKR method, which makes use of expansions and integration within a single unit cell only. The lattice sums in equations (77) do not have convenient convergence properties, as they depend on the tails of the Wannier functions in real space. Important to note is the fact that the phase freedom of the Bloch states allows for an optimization of these tails to reduce the numerical effort. By now an efficient procedure giving ‘maximally localized’ Wannier functions [29, 30] has been developed to deal with this issue. Interestingly, in this procedure matrix elements of both $\nabla_{\mathbf{k}}$ and \mathbf{r} , as in the KKR method discussed in section 2.1, occur. Reassuringly, it is found that in both approaches an easy to evaluate matrix element of $\nabla_{\mathbf{k}}$ dominates over what is frequently called the dipole contribution involving matrix elements of \mathbf{r} . The Wannier orbitals are localized but, unlike the orbitals in the tight-binding method, exact representations of the band structure of a periodic solid within this method are possible only for a limited energy range. For metals, its use in modern first-principle calculations is based on the unique ‘maximally localized orbitals’ and its power and achievements are well summarized in [29]. Here we wish to recall only the bare outline of the new development occasioned by the current interest in the geometrical and topological features of the electronic structure of crystals.

The method based on the Wannier interpolation scheme, fully described in [21], starts with a conventional DFT calculation of Bloch states $|\Psi_{n\mathbf{q}}\rangle$ in a certain energy range and on a selected mesh of \mathbf{q} points based on a plane-wave expansion. Then the matrix elements of various operators may be constructed with respect to a set of maximally localized Wannier states $|\mathbf{R}n\rangle$. It should be mentioned that generally these states are distinct from the Wannier states defined in equation (76) since they are solutions of a procedure to minimize the real space spread of the Wannier functions [30]. The minimization is always possible due to the freedom choosing an arbitrary phase in the definition of Bloch states as mentioned above. In general, this freedom in defining the Bloch states can be written in terms of a unitary operator. If we assume a set of Wannier states chosen according to this procedure, the phase sum of these states

$$\langle \mathbf{r} | u_n^W(\mathbf{k}) \rangle = \sum_{\mathbf{R}} e^{-i\mathbf{k}\cdot(\mathbf{r}-\mathbf{R})} \langle \mathbf{r} | \mathbf{R}n \rangle \quad (78)$$

can be defined for an arbitrary \mathbf{k} point, which may be at or in between the first-principle \mathbf{q} -point mesh. It can be regarded as a ‘Wannier gauge’ representation of the periodic part of a Bloch state but they are generally no eigenstates of the \mathbf{k} -dependent Hamiltonian. In the following one has to evaluate the matrix elements with respect to the constructed states

$$\begin{aligned} H_{nm}^W(\mathbf{k}) &= \sum_{\mathbf{R}} e^{+i\mathbf{k}\cdot\mathbf{R}} \langle 0n | \hat{H} | \mathbf{R}m \rangle, \\ \nabla H_{nm}^W(\mathbf{k}) &= \sum_{\mathbf{R}} e^{+i\mathbf{k}\cdot\mathbf{R}} i\mathbf{R} \langle 0n | \hat{H} | \mathbf{R}m \rangle, \\ \mathbf{A}_{nm}^W(\mathbf{k}) &= \sum_{\mathbf{R}} e^{+i\mathbf{k}\cdot\mathbf{R}} \langle 0n | \mathbf{r} | \mathbf{R}m \rangle, \\ \Omega_{nm}^W(\mathbf{k}) &= i \sum_{\mathbf{R}} e^{+i\mathbf{k}\cdot\mathbf{R}} \langle 0n | \mathbf{R} \times \mathbf{r} | \mathbf{R}m \rangle. \end{aligned} \quad (79)$$

Actually, all of them are given in the same ‘Wannier gauge’. The indices n and m refer to the full bundle of Wannier states selected to represent the real bands up to a certain energy above the Fermi level.

The next step is to find unitary matrices $\bar{U}(\mathbf{k})$ such that

$$\begin{aligned} \bar{U}^\dagger(\mathbf{k}) \bar{H}^W(\mathbf{k}) \bar{U}(\mathbf{k}) &= \bar{H}^H(\mathbf{k}) \quad \text{with} \\ H_{nm}^H(\mathbf{k}) &= \mathcal{E}_{n\mathbf{k}} \delta_{nm}, \end{aligned} \quad (80)$$

where the eigenvalues $\mathcal{E}_{n\mathbf{k}}$ should agree with the first-principle dispersion relation of the bands chosen to be represented. The corresponding eigenfunctions

$$|u_n^H(\mathbf{k})\rangle = \sum_m U_{nm}(\mathbf{k}) |u_m^W(\mathbf{k})\rangle \quad (81)$$

should reproduce the periodic part of these states.

Thus, $|u_n^H(\mathbf{k})\rangle$ can be used to evaluate equations (20) and (21) for the Berry connection and the curvature in the standard way. However, such direct calculations are precisely not what one would like to do. The point of Wang *et al* is that the above preamble offers an alternative. Namely, the unitary transformation $\bar{U}(\mathbf{k})$ transforms all states and operators from the ‘Wannier gauge’ to another gauge which is called the ‘Hamiltonian (H) gauge’ and one can transform all the easy to evaluate ‘Wannier gauge’ operators in equation (79) into their ‘Hamiltonian gauge’ form. Of course, $\Omega_{nm}^H(\mathbf{k})$ is of particular interest. Unfortunately, due to the \mathbf{k} dependence of $U_{nm}(\mathbf{k})$ the form of equations (20) and (21) is not covariant under such a transformation. For instance, the connection is given by

$$\mathbf{A}^H = U^\dagger \mathbf{A}^W U + iU^\dagger \nabla U = \bar{\mathbf{A}}^H + iU^\dagger \nabla U, \quad (82)$$

where for clarity the momentum dependency has been dropped as we will mainly do within this section. All products are matrix multiplications and the gradient is taken with respect to \mathbf{k} . A similar, but more complicated formula can be derived for Ω^H . The matrices $\bar{\mathbf{A}}^H$, $\bar{\Omega}^H$, and \bar{H}^H denote the covariant components, that is to say the part of the transformed operator which does not contain $U^\dagger \nabla U$, of \mathbf{A}^H and H^H , respectively. If we write $\bar{\Omega}^H = U^\dagger \Omega^W U$ and

$$\mathbf{D}_{nm}^H = (U^\dagger \nabla U)_{nm} = \frac{(U^\dagger \nabla H^W U)_{nm}}{\mathcal{E}_m - \mathcal{E}_n} (1 - \delta_{nm}), \quad (83)$$

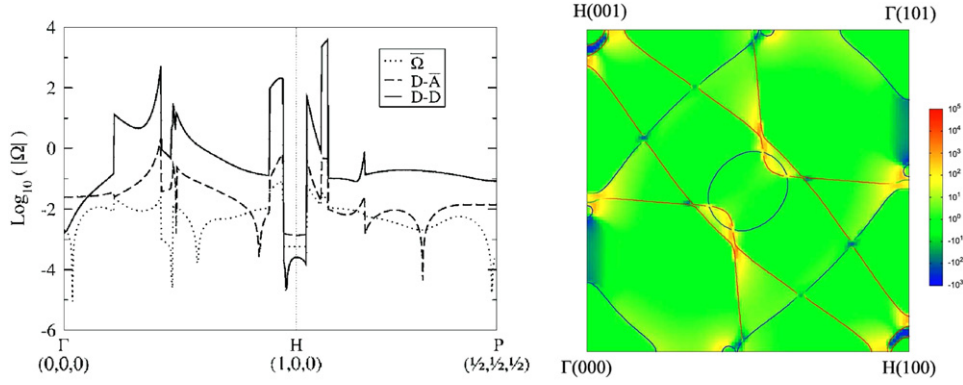


Figure 13. Left: Berry curvature $\Omega^z(\mathbf{k})$ of Fe along symmetry lines with a decomposition into three different contributions of equation (84) (note the logarithmic scale). Right: Fermi surface in the (010) plane (solid lines) and the total Berry curvature $-\Omega^z(\mathbf{k})$ in atomic units (color map). Reproduced with permission from [21]. Copyright 2006 American Physical Society.

the final formula for the *total* Berry curvature $\Omega(\mathbf{k}) = \sum_n f_n \Omega_n(\mathbf{k})$, including the sum over all occupied states, reads as follows:

$$\Omega(\mathbf{k}) = \sum_n f_n \bar{\Omega}_{nm}^H + \sum_{n,m} (f_m - f_n) \mathbf{D}_{nm}^H \times \bar{\mathbf{A}}_{mn}^H + \Omega^{DD}, \quad (84)$$

where the last term takes the form

$$\Omega^{DD} = i/2 \sum_{n,m} (f_n - f_m) \frac{(U^\dagger \nabla H^W U)_{nm} \times (U^\dagger \nabla H^W U)_{mn}}{(\mathcal{E}_m - \mathcal{E}_n)^2}. \quad (85)$$

Here $f_n \equiv f_n(\mathbf{k})$ and $f_m \equiv f_m(\mathbf{k})$ are the equilibrium distribution functions for bands n and m , respectively. The sums in equation (84) run over all Wannier states used for an accurate description of the occupied states. Interestingly, this is the standard form of the Berry curvature for a Hamiltonian which depends parametrically on \mathbf{k} and it also shows up as one of the contributions in the KKR and the tight-binding approaches discussed in sections 2.1 and 2.2. Reassuringly, computations by all three methods find the contribution from such terms as equation (85) dominant and almost exclusively responsible for the spiky features as functions of \mathbf{k} . As noted in the introduction, these features originate from band crossings or avoided crossings and have a variety of interesting physical consequences.

For instance, the Berry curvature calculated by Wang *et al* [21, 31], shown in figure 13, leads directly to a good quantitative account of the intrinsic contribution to the anomalous Hall effect in Fe. The left panel of figure 13 shows the decomposition of the Berry curvature in different contributions arising from the expansion of the states into a Wannier basis (see equation (84)). Noting the logarithmic scale, it is evident that the dominant contribution stems from the Berry curvature $\Omega^{DD}(\mathbf{k})$ of the \mathbf{k} -dependent Hamiltonian $\bar{H}^H(\mathbf{k})$ according to equation (85). The other terms including matrix elements of the position operator \mathbf{r} are negligible, which is similar to what turned out to be the case within the KKR method. Further applications of the considered method to the cases of fcc Ni and hcp Co [31, 32] are equally impressive.

2.4. Kubo formula

2.4.1. Anomalous Hall conductivity and the Berry curvature.

Most conventional approaches to the electronic transport in solids are based on the very general linear response theory of Kubo [33]. Indeed, the first insight into the cause of the anomalous Hall effect by Karplus and Luttinger [34] was gained by deploying the Kubo formula for a simple model Hamiltonian of electrons with spin. In this section we review briefly the first-principle implementation of the Kubo formula in aid of calculating the Berry curvature. The simple observation which makes this possible is that both the semiclassical description and the Kubo formula approach yield the same expression for the intrinsic contribution to the anomalous Hall conductivity (AHC). Hence, by comparing the two, a Kubo-like expression for the Berry curvature can be extracted. Here we examine the formal connection between the two formulas for the Berry curvature and demonstrate that they are equivalent, as was mentioned already by Wang *et al* [21].

The Kubo formula for the AHC in the static limit for disorder-free noninteracting electrons is given by [35]

$$\sigma_{xy} = e^2 \hbar \int_{BZ} \frac{d^3 k}{(2\pi)^3} \sum_n \sum_{m \neq n} f_n(\mathbf{k}) \times \frac{\text{Im}[\langle \Psi_{n\mathbf{k}} | \hat{v} | \Psi_{m\mathbf{k}} \rangle \times \langle \Psi_{m\mathbf{k}} | \hat{v} | \Psi_{n\mathbf{k}} \rangle]_z}{(\mathcal{E}_{n\mathbf{k}} - \mathcal{E}_{m\mathbf{k}})^2}, \quad (86)$$

whereas in the semiclassical approach it is expressed in terms of the Berry curvature [7, 14, 34, 41]

$$\sigma_{xy} = -\frac{e^2}{\hbar} \sum_n \int_{BZ} \frac{d^3 k}{(2\pi)^3} f_n(\mathbf{k}) \Omega_n^z(\mathbf{k}). \quad (87)$$

Assuming the equivalence of the two approaches, a comparison of equations (86) and (87) yields a Kubo-like formula for the Berry curvature. However, the equivalence is not a priori evident and has to be proven, which will be done in the following.

The starting point is the Berry curvature written in terms of the periodic part of the Bloch function

$$\Omega_n(\mathbf{k}) = i \langle \nabla_{\mathbf{k}} u_n(\mathbf{k}) | \times | \nabla_{\mathbf{k}} u_n(\mathbf{k}) \rangle. \quad (88)$$

Let us follow the route given by Berry [3] to rewrite this expression. Introducing the completeness relation with respect to the N present bands, $1 = \sum_{m=1}^N |u_m\rangle\langle u_m|$, excluding the vanishing term with $m = n$ and using the relation

$$\langle \nabla u_n(\mathbf{k}) | u_m(\mathbf{k}) \rangle = \frac{\langle u_n(\mathbf{k}) | \nabla_{\mathbf{k}} H(\mathbf{k}) | u_m(\mathbf{k}) \rangle}{\mathcal{E}_{n\mathbf{k}} - \mathcal{E}_{m\mathbf{k}}}, \quad (89)$$

which follows from $\langle u_n(\mathbf{k}) | H(\mathbf{k}) | u_m(\mathbf{k}) \rangle = \mathcal{E}_{m\mathbf{k}} \langle u_n(\mathbf{k}) | u_m(\mathbf{k}) \rangle = 0$, yields

$$\Omega_n(\mathbf{k}) = i \sum_{m \neq n} \frac{\langle u_n(\mathbf{k}) | \nabla_{\mathbf{k}} H(\mathbf{k}) | u_m(\mathbf{k}) \rangle \times \langle u_m(\mathbf{k}) | \nabla_{\mathbf{k}} H(\mathbf{k}) | u_n(\mathbf{k}) \rangle}{(\mathcal{E}_{n\mathbf{k}} - \mathcal{E}_{m\mathbf{k}})^2}. \quad (90)$$

If we reformulate it with respect to the Bloch functions

$$\begin{aligned} \Omega_n(\mathbf{k}) = & i \sum_{m \neq n} \{ \langle \Psi_{n\mathbf{k}} | e^{i\mathbf{k}\mathbf{r}} \nabla_{\mathbf{k}} H(\mathbf{k}) e^{-i\mathbf{k}\mathbf{r}} | \Psi_{m\mathbf{k}} \rangle \\ & \times \langle \Psi_{m\mathbf{k}} | e^{i\mathbf{k}\mathbf{r}} \nabla_{\mathbf{k}} H(\mathbf{k}) e^{-i\mathbf{k}\mathbf{r}} | \Psi_{n\mathbf{k}} \rangle \} \\ & \times \{ (\mathcal{E}_{n\mathbf{k}} - \mathcal{E}_{m\mathbf{k}})^2 \}^{-1} \end{aligned} \quad (91)$$

and use the relations

$$H(\mathbf{k}) = e^{-i\mathbf{k}\mathbf{r}} \hat{H} e^{i\mathbf{k}\mathbf{r}}, \quad (92)$$

$$\nabla_{\mathbf{k}} H(\mathbf{k}) = i e^{-i\mathbf{k}\mathbf{r}} \left[\hat{H} \mathbf{r} - \mathbf{r} \hat{H} \right] e^{i\mathbf{k}\mathbf{r}} = \hbar e^{-i\mathbf{k}\mathbf{r}} \hat{\mathbf{v}} e^{i\mathbf{k}\mathbf{r}}, \quad (93)$$

we end up with a Kubo-like formula widely used in the literature [37, 38]

$$\Omega_n(\mathbf{k}) = i \hbar^2 \sum_{m \neq n} \frac{\langle \Psi_{n\mathbf{k}} | \hat{\mathbf{v}} | \Psi_{m\mathbf{k}} \rangle \times \langle \Psi_{m\mathbf{k}} | \hat{\mathbf{v}} | \Psi_{n\mathbf{k}} \rangle}{(\mathcal{E}_{n\mathbf{k}} - \mathcal{E}_{m\mathbf{k}})^2}. \quad (94)$$

This formula proves the equivalence of the two approaches for calculating the AHC as given by equations (86) and (87). In principle, all occupied and unoccupied states have to be accounted for in the sum of equation (94). However, in practice only states with energies close to $\mathcal{E}_{n\mathbf{k}}$ play a role. An important feature of this form is that it is expressed in terms of the off-diagonal matrix elements of the velocity operator with respect to the Bloch states. To deal with them a technique was adopted, which served well for computing the optical conductivities [39, 40], where the same matrix elements have been required.

The first *ab initio* calculation of the Berry curvature was actually performed for SrRuO₃ by Fang *et al* [36] using equation (94). The authors nicely illustrate the existence of a magnetic monopole in the crystal momentum space, which is shown in figure 14. The origin of this sharp structure is the near degeneracy of bands. It acts as a magnetic monopole. A similar effect was found for Fe by Yao *et al* [41]. They demonstrate that for \mathbf{k} points near the spin-orbit driven avoided crossings of the bands the Berry curvature is extremely enhanced as shown in figure 15. In addition, the agreement between the right panels of figures 13 and 15 shows impressively the equivalence between the two different methods.

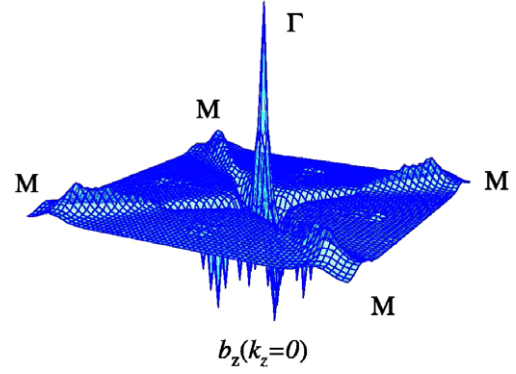


Figure 14. Calculated Berry curvature (in [36] called flux b_z) $\Omega^z(\mathbf{k}) = \sum_{n \in \{t_{2g}\}} \Omega_n^z(\mathbf{k})$ distribution in \mathbf{k} space for t_{2g} bands as a function of (k_x, k_y) with $k_z = 0$ for SrRuO₃ with cubic structure. Reproduced with permission from [36]. Copyright 2003 AAAS.

2.4.2. Spin Hall conductivity and the Berry curvature. Of course, the fact that the results of the semiclassical transport theory and the quantum mechanical Kubo formula agree exactly, as was shown above, is surprising. In general, it cannot be expected for all transport coefficients. Indeed, as we shall now demonstrate, the situation is quite different for the spin Hall conductivity.

Evidently, the Kubo approach is readily adopted to calculate the spin-current response to an external electric field \mathbf{E} . Although there is still a controversy about an expression for the spin-current operator to be taken [42–45], frequently the following tensor product of the relativistic spin operator $\hat{\beta} \hat{\Sigma}$ and the velocity operator $\hat{\mathbf{v}}$ is used:

$$\hat{\mathbf{J}}^{\text{Spin}} = \hat{\beta} \hat{\Sigma} \otimes \hat{\mathbf{v}}, \quad \hat{\beta} \hat{\Sigma} = \begin{pmatrix} \hat{\boldsymbol{\sigma}} & 0 \\ 0 & -\hat{\boldsymbol{\sigma}} \end{pmatrix}. \quad (95)$$

Furthermore, the symmetrized version of the tensor product is often used in literature and the spin-current response is calculated as the expectation value of the operator $\hat{\mathbf{J}}^{\text{Spin}}$. However, within the Dirac approach we have

$$\begin{aligned} \hat{\mathbf{v}} = c \hat{\boldsymbol{\alpha}} = c \begin{pmatrix} 0 & \hat{\boldsymbol{\sigma}} \\ \hat{\boldsymbol{\sigma}} & 0 \end{pmatrix} \quad \text{and} \\ \hat{\beta} \hat{\Sigma}_i \hat{\mathbf{v}}_j - \hat{\mathbf{v}}_j \hat{\beta} \hat{\Sigma}_i = 0, \quad \text{if } i \neq j. \end{aligned} \quad (96)$$

Similar to the formula for the charge Hall conductivity, one finds for the spin Hall conductivity with spin polarization in the z direction [43, 37, 38]

$$\sigma_{xy}^z = \frac{e^2}{\hbar} \sum_{\mathbf{k}, n} \sigma_{xy;n}^z(\mathbf{k}) f_n(\mathbf{k}), \quad (97)$$

where the \mathbf{k} and band resolved conductivity $\sigma_{xy;n}^z(\mathbf{k})$ in the framework of the Kubo formula (Kubo) is given by

$$\begin{aligned} \sigma_{xy;n}^z(\mathbf{k})_{\text{Kubo}} = \\ - \hbar^2 \sum_{m \neq n} \frac{\text{Im}[\langle \Psi_{n\mathbf{k}} | \hat{\beta} \hat{\Sigma}_z \hat{\mathbf{v}}_x | \Psi_{m\mathbf{k}} \rangle \langle \Psi_{m\mathbf{k}} | \hat{\mathbf{v}}_y | \Psi_{n\mathbf{k}} \rangle]}{(\mathcal{E}_{n\mathbf{k}} - \mathcal{E}_{m\mathbf{k}})^2}. \end{aligned} \quad (98)$$

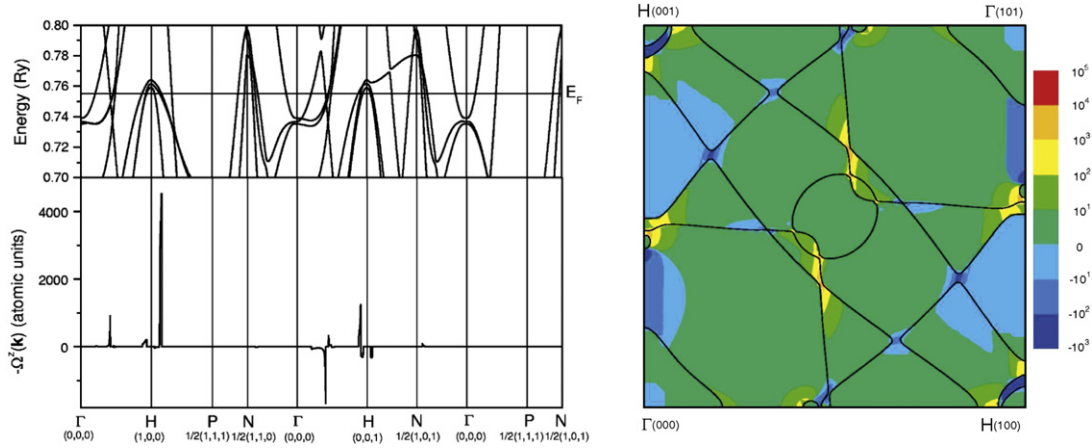


Figure 15. Left: band structure of bulk Fe near Fermi energy (upper panel) and Berry curvature $\Omega^z(\mathbf{k})$ (lower panel) along symmetry lines. Right: Fermi surface in (010) plane (solid lines) and Berry curvature $-\Omega^z(\mathbf{k})$ in atomic units (color map). Reproduced with permission from [41]. Copyright 2004 American Physical Society.

In the literature, this quantity is sometimes even called spin Berry curvature [38], analogously to the AHE. This notation is misleading and should not be used.

Let us tackle the same problem from the point of view of the semiclassical theory (sc). This suggests that one should take the velocity in equations (95) to be the anomalous velocity given by equation (11). This argument leads to [5, 42]

$$\sigma_{xy;n}^z(\mathbf{k})_{\text{sc}} = \text{Tr}[\bar{S}_n^z(\mathbf{k})\bar{\Omega}_n^z(\mathbf{k})]. \quad (99)$$

Here $(\bar{S}_n^z(\mathbf{k}))_{ij} = \langle \Psi_{ni\mathbf{k}} | \hat{\beta} \hat{\Sigma}_z | \Psi_{nj\mathbf{k}} \rangle$ is the spin matrix for a Kramers pair labeled by i, j and $\bar{\Omega}_n^z(\mathbf{k})$ is the non-Abelian Berry curvature [19] introduced in section 1.3. The point we wish to make here is that this formula is not equivalent to the Kubo form in equation (98). The reason is that the band off-diagonal terms of the spin matrix were neglected in the derivation from the wave packet dynamics of equation (99) [5].

Evidently, $\sigma_{xy;n}^z(\mathbf{k})_{\text{Kubo}}$ cannot be written as a single-band expression, in contrast to the case of the AHC, which turned out to be exactly the conventional Berry curvature (see section 2.4.1). The contributions of equation (98) which were neglected in equation (99) are of quantum mechanical origin and are not accounted for in the semiclassical derivation. Culcer *et al* [42] tackled the problem and identified the neglected contributions, without giving up the wave packet idea, as spin and torque dipole terms. Nevertheless, it was shown that under certain approximations a semiclassical description may result in quantitatively comparable results to the Kubo approach [19]. This will be discussed in section 3.

3. Intrinsic contribution to the charge and spin conductivity in metals

Here we discuss applications of the computational methods for the Berry curvature discussed in section 2. We will focus on first-principle calculations of the anomalous and spin Hall

conductivities. The anomalous Nernst conductivity, closely related to it, will be also discussed briefly.

The first *ab initio* studies of the AHE, based on equation (87) with $\Omega_n(\mathbf{k})$ defined by equation (94), were reported in [36, 46]. As is well known, the conventional expression for the Hall resistivity

$$\rho_{xy} = R_0 B_z + 4\pi R_s M_z \quad (100)$$

(where B_z is the magnetic field in the z direction and R_0 and R_s are the normal and the anomalous Hall coefficient, respectively) assumes a monotonic behavior of ρ_{xy} as well as σ_{xy} as a function of the magnetization M . By means of first-principle calculations based on the pseudopotential method (STATE code), Fang *et al* [36] have shown that the unconventional nonmonotonic behavior of the AHC measured in SrRuO₃ (figure 16, left) is induced by the presence of a magnetic monopole (MM) in momentum space (see figure 14 and the corresponding discussion in section 2.4.1). The existence of MMs causes the sharp and spiky structure of the AHC as a function of the Fermi-level position, shown in the right panel of figure 16. At the self-consistently determined Fermi level, the calculated value $\sigma_{xy} = -60 (\Omega \text{ cm})^{-1}$ is comparable with the experimentally observed conductivity of about $-100 (\Omega \text{ cm})^{-1}$. Obviously, a small change in the Fermi level would cause dramatic changes in the resulting AHC. Indeed, as was shown in [46], the calculated AHC of ferromagnetic Gd₂Mo₂O₇ and Nd₂Mo₂O₇ is strongly changed by the choice of the Coulomb repulsion U varied in the used mean-field Hartree–Fock approach.

A year later, results for the intrinsic AHC in ferromagnetic bcc Fe, based on the full-potential linearized augmented plane-wave method (WIEN2K code), were published [41]. The authors used the same Kubo formula approach to describe the transversal transport. In particular, a close agreement between theory, $\sigma_{xy} = 751 (\Omega \text{ cm})^{-1}$, and experiment, $\sigma_{xy} = 1032 (\Omega \text{ cm})^{-1}$, was found, that points to the dominance of the intrinsic contribution in Fe. A slow convergence of the calculated value for the AHC with respect to the number of \mathbf{k} points was reported. The reason for the convergence

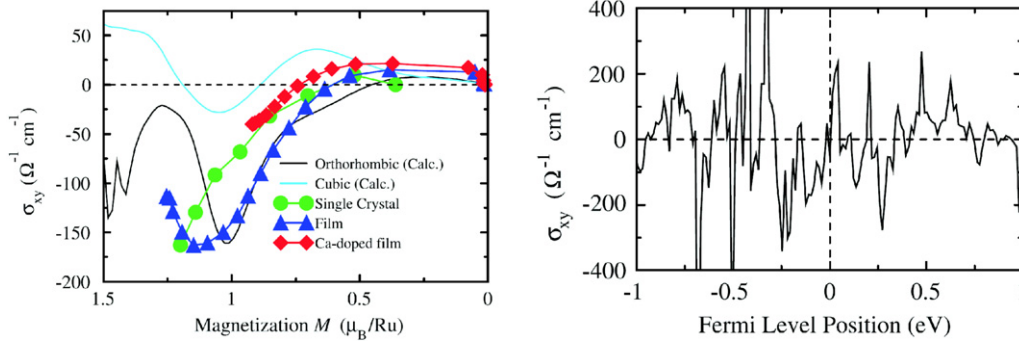


Figure 16. Left: the Hall conductivity σ_{xy}^z of SrRuO₃ as a function of the magnetization along z . Right: σ_{xy}^z , as a function of the Fermi-level position for the orthorhombic structure of SrRuO₃. Reproduced with permission from [36]. Copyright 2003 AAAS.

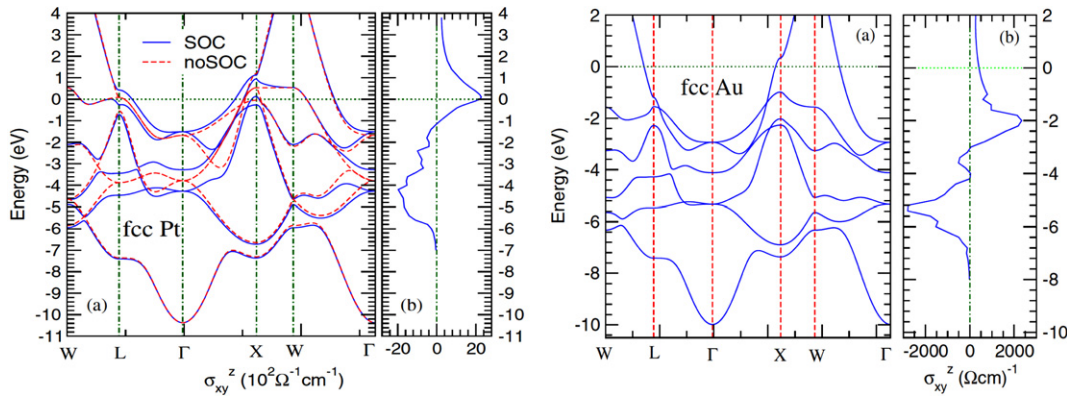


Figure 17. Left, (a) relativistic band structure and (b) spin Hall conductivity for variable Fermi level of fcc Pt (reproduced with permission from [47]. Copyright 2008 American Physical Society); right, (a) relativistic band structure and (b) spin Hall conductivity of fcc Au (reproduced with permission from [48]. Copyright 2009 American Institute of Physics). The dashed curves in the left panel represent the scalar-relativistic band structure. The real Fermi level is set as the zero of the energy scale.

problems is given by small regions in momentum space around avoided crossings and enhanced spin-orbit coupling. In the behavior of the Berry curvature these points cause strong peaks, which is shown in figure 15. If both related states of the avoided crossing are occupied, their combined contribution to the AHC is negligible since they compensate each other. However, when the Fermi level lies in a spin-orbit induced gap, the occupied state, which acts now as an isolated magnetic monopole, causes a peak in the AHC. Consequently, it was necessary to use millions of \mathbf{k} points in the first Brillouin zone to reach convergence.

To avoid such demanding computational efforts, the Wannier interpolation scheme, discussed in section 2.3, was suggested and applied for Fe in [21]. The authors started with the relativistic electronic structure obtained by the pseudopotential method (PWSCF code) at a relatively coarse \mathbf{k} mesh. Using maximally localized Wannier functions, constructed from the obtained Bloch states, all quantities of interest were expressed in the tight-binding like basis and interpolated onto a dense \mathbf{k} mesh. Finally, this new mesh was used to calculate the AHC. The obtained value of $756 (\Omega \text{cm})^{-1}$ is in good agreement with the result of [41].

The same scheme was used further on to calculate the AHC applying Haldane’s formula [16] which means integration not over the entire Fermi sea, as is required by

the Kubo formula, but only over the Fermi surface. The results obtained for Fe, Co, and Ni [31] agreed very well for both procedures and with previous theoretical studies [41]. Moreover, the work done by the group of Vanderbilt [21] has stimulated further first-principle calculations as will be shown below. The first *ab initio* calculations of the spin Hall conductivity (SHC) were performed for semiconductors and metals [37, 38]. The description of the electronic structure in [38] was based on the full-potential linearized augmented plane-wave method (WIEN2K code) and in [37] on the all-electron linear muffin-tin orbital method, but both rely on the solution of the Kubo formula given by equation (98) to describe the SHC. Later, in [47] the relatively large SHC measured in Pt was explained by the contribution of the spin-orbit split d bands at the high-symmetry points L and X near the Fermi level (figure 17, left). In contrast, Au [48] shows similar contributions to the SHC, but at lower energies with respect to the Fermi level E_F , since the extra electron of Au with respect to Pt causes full occupation of the d bands (figure 17, right).

The spin-orbit coupling is the origin of the AHE and the SHE. In particular, the avoided crossings significantly increase these effects. In addition, the spin-orbit coupling links the spin degree of freedom to the crystal lattice, which is the source of the anisotropy with respect to

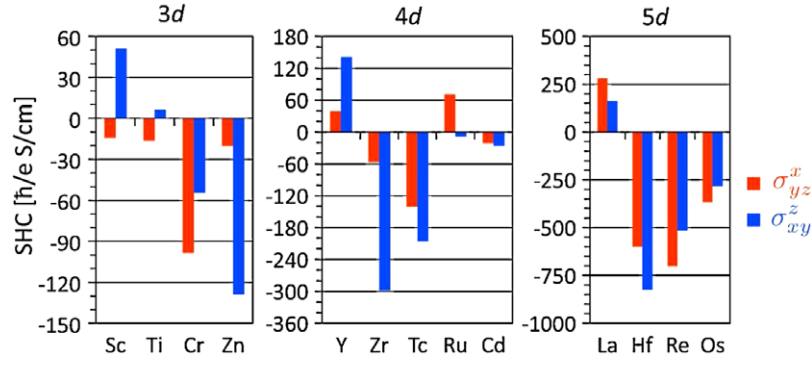


Figure 18. Spin Hall conductivities σ_{yz}^x and σ_{xy}^z for several hcp nonmagnetic metals and for antiferromagnetic Cr. Reproduced with permission from [49]. Copyright 2010 American Physical Society.

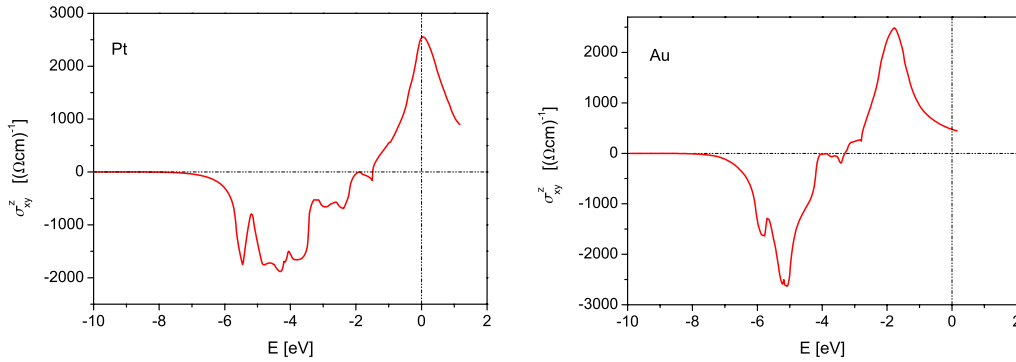


Figure 19. The intrinsic spin Hall conductivity for fcc Pt (left) and Au (right) [19]. The Fermi level is set to zero on the energy scale. Reproduced with permission from [19]. Copyright 2011 American Physical Society.

the chosen quantization axis; this means σ_{yz}^x and σ_{xy}^z may differ. This was demonstrated first for the AHE in hcp Co [32] and later for the SHE in several nonmagnetic hcp metals [49] (figure 18). Here, the pseudopotential method (PWSCF code) and the full-potential linearized augmented plane-wave method (FLEUR code) were used for the AHE and SHE, respectively. To reduce the computational efforts, the Berry curvature calculations were based on the Wannier interpolation scheme according to [21]. These methods were applied to several situations in ordered alloys [50] where the anisotropy of the AHC [51] was discussed as well and the roles of spin-conserving and non-spin-conserving parts of the SOC were discussed in detail [52]. Very recently the same group calculated the scattering-independent contribution to the side jump mechanism for the anomalous Hall effect [53]. The used approach is based on a model assuming short-range uncorrelated disorder and involves the Berry connection of the Bloch states as an essential part [54].

Finally, an approach for calculating the SHC based on the KKR method was proposed ([19], section 2.1). For the description of the transversal spin transport the authors applied an approach different from the widely used Kubo formula. Their calculations are based on the expression for the SHC in the non-Abelian case suggested in [5]. This expression was simplified further by the approximation that the expectation value of the $\hat{\beta}\hat{\Sigma}_z$ operator is assumed to be +1 and -1 for the two spin degenerate states, arising

in nonmagnetic crystals with inversion symmetry. Thus, the semiclassical treatment was reduced to the two current model with the final expression for the SHC in terms of the usual formula for the AHC at zero temperature

$$\sigma_{xy}^z = \frac{e^2}{\hbar(2\pi)^3} \int^{E_F} d\mathcal{E} \Omega^z(\mathcal{E}), \quad (101)$$

where $\Omega^z(\mathcal{E})$ is defined by equation (65). The spin Hall conductivities $\sigma_{xy}^z(\mathcal{E})$ considered for a variable Fermi level, and calculated for Pt and Au in such an approach (figure 19), are quantitatively in good agreement with the ones obtained by the Kubo-like formula (see figure 17).

Related to the already discussed calculation of the intrinsic spin and anomalous Hall conductivities is the intrinsic mechanism of the anomalous Nernst effect. It is driven by an applied thermal gradient instead of the applied electric field. The two driving forces are of physically different nature. The electric field is a mechanical force in contrast to the statistical force of a temperature gradient. Nevertheless, as was shown by Xiao *et al* [55], the final expression for the anomalous Nernst conductivity α_{xy} at low temperatures is simply given by the Mott relation

$$\alpha_{xy} = \frac{\pi^2 k_B^2 T}{3e} \sigma'_{xy}(E_F). \quad (102)$$

Here $\sigma'_{xy}(E_F)$ is the first energy derivative at E_F of the intrinsic anomalous Hall conductivity, defined in terms of

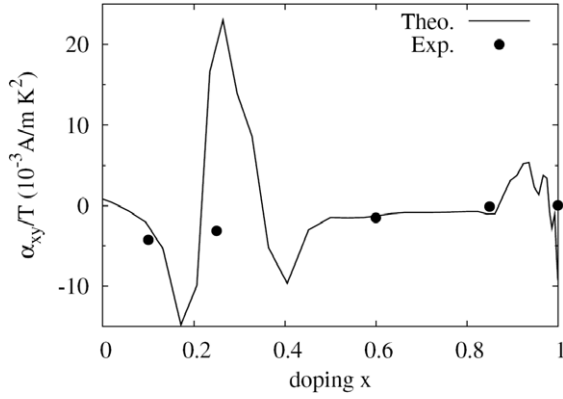


Figure 20. The intrinsic anomalous Nernst conductivity (divided by the temperature T) of the $\text{CuCr}_2\text{Se}_{4-x}\text{Br}_x$ alloy as a function of the Br content x . Reproduced with permission from [55]. Copyright 2006 American Physical Society.

the Berry curvature in equation (87). All the above methods to calculate the Berry curvature can be applied to compute the anomalous Nernst conductivity as well. In figure 20 a comparison between experimental results and first-principle calculations for the alloy $\text{CuCr}_2\text{Se}_{4-x}\text{Br}_x$ are shown. The concentration dependence is described by using a rigid band model. The agreement is relatively good despite the fact that the experiment cannot resolve the peak–valley structure around $x = 0.2$.

4. De Haas–van Alphen oscillation and the Berry phases

Other phenomena related to the topic of this review are various quantum oscillations. For their proper description typically the Berry phase accumulated along a closed orbit in parameter space is needed, which can be expressed via the Berry curvature of the system. For instance, in the case of the de Haas–van Alphen effect, the semiclassical formula for the quantized energies of the Landau levels includes a term involving the Berry phase of the corresponding orbits in \mathbf{k} space. This was pointed out by Mikitik and Sharlai [56, 57], who have discussed a number of interesting experiments in these terms [58, 59]. They argue that the quasiparticles which move along closed orbits in response to an external magnetic field \mathbf{B} are wave packets, in the sense of the semiclassical theory, and therefore their semiclassical equations (8) and (9) are subject to corrections arising from Berry phases and curvatures. In short, a closed orbit is defined by the requirement that the energy of the wave packet $\mathcal{E}_{n\mathbf{k}} - \mathbf{M}(\mathbf{k})\mathbf{B}$ is equal to $E = \text{constant}$ for all \mathbf{k} along the orbit. Here $\mathbf{M}(\mathbf{k})$ is the spin plus the orbital magnetic moment of the electron along the path. Then the Bohr–Sommerfeld quantization condition for $E = E_v$ to be a Landau level is [1, 57, 60]

$$S(E_v, k_z) = 2\pi\hbar e B_z \left(\nu + \frac{1}{2} - \frac{\gamma_n}{2\pi} \right), \quad (103)$$

where $S(E_v, k_z)$ is the area enclosed by the orbit in \mathbf{k} space. The Berry phase accumulated along the orbit labeled by C is

given by

$$\gamma_n = \oint_C d\mathbf{k} \cdot \mathbf{A}_n(\mathbf{k}) = \iint_{S_C} d\mathbf{S} \cdot \boldsymbol{\Omega}_n(\mathbf{k}), \quad (104)$$

where S_C is any surface in \mathbf{k} space whose boundary is C . Clearly, the presence of the orbital magnetization in the theory indicates that the change of the band energy due to spin and orbital motion is taken into account. This important fact is more evident if equation (103) is recast as

$$S_0(\mathcal{E}_{n\mathbf{k}}, k_z) = 2\pi\hbar e B_z \times \left(\nu + \frac{1}{2} - \frac{\gamma_n}{2\pi} - \frac{1}{2\pi} \oint_{C_0} \frac{M_z(k) d\mathbf{k}}{|\partial \mathcal{E}_{n\mathbf{k}} / \partial k_{\perp}|} \right), \quad (105)$$

where $S_0(\mathcal{E}_{n\mathbf{k}}, k_z)$ is the area enclosed by an orbit C_0 on an iso-energetic surface of the actual band structure. From the point of view of analyzing the high quality data available from de Haas–van Alphen measurements, the physical content of the above formula is of considerable general interest, and shows the necessary correction of the common theory. However, to calculate the loop integral in equation (105) for the general case with spin–orbit coupling is a real challenge, which has been, so far, only partially implemented⁶.

The full theory has already been presented by Roth in 1966 [61], although never applied to analyze experimental data. Only recently the formulas have been revisited in view of the new light cast on them by advances in describing wave packets driven by external fields and the associated Berry phases.

To highlight the significance of the Berry phase and curvature in the present context, we shall now consider the simple case where the spin, and therefore the spin–orbit coupling, is altogether neglected and it is assumed that the system is time-reversal and inversion symmetric. In this case one might think that the Berry phase would vanish since the Berry curvature is zero over the full Brillouin zone. However, as was shown by Mikitik and Sharlai [56, 57], this is not true if the semiclassical orbit encloses a line of degeneracy. As was shown in [58, 59] for several materials, such lines exist in the absence of spin–orbit coupling and have a significant effect on the observable de Haas–van Alphen frequencies.

Here we focus on two hexagonal systems, Mg and Tl, and discuss the results for γ_n , given by equation (104), obtained with the KKR method [22, 19]. In figure 21 the band structure of Mg along the ΓM direction clearly shows an accidental degeneracy, which is actually part of a full line in the $k_z = 0$ plane as shown in the right panel of figure 21. Furthermore, this line is enclosed by one sheet of the Fermi surface, which allows us to study the effect. If the magnetic field is applied in different directions as shown in figure 22, orbits either enclose the line of degeneracy, as in the case shown in red, or they do not, shown in black. We have evaluated the integrals over a selection of those loops numerically and found $\gamma_n = \pi$ for all orbits which enclose the line and $\gamma_n = 0$ for all those which do not. The important fact is that the integral value

⁶ See for example [63] and citations [9–30] in [62].

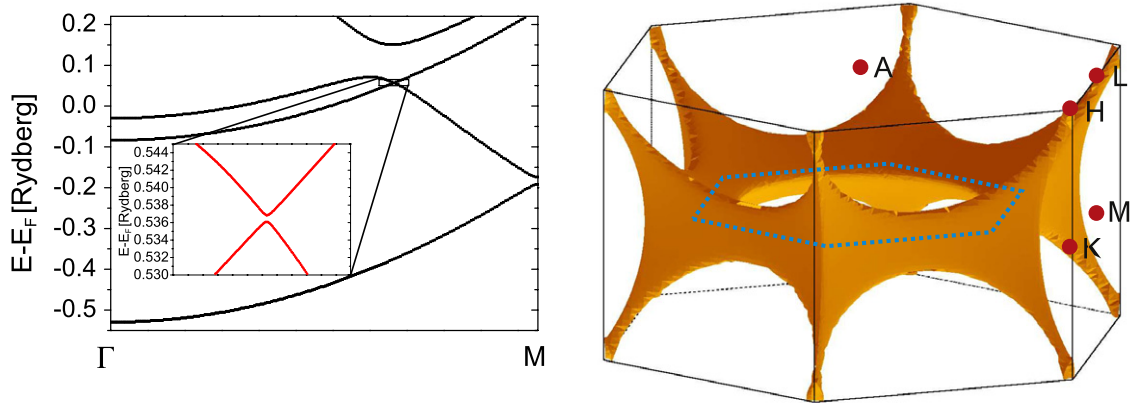


Figure 21. Left panel: band structure of hcp Mg along the Γ M direction. The accidental degeneracy of two bands is part of a line of degeneracy in the $k_z = 0$ plane. The inset shows the lifting of the degeneracy due to spin-orbit coupling. Right panel: the full line of degeneracy which is enclosed by the Fermi surface of the second band.

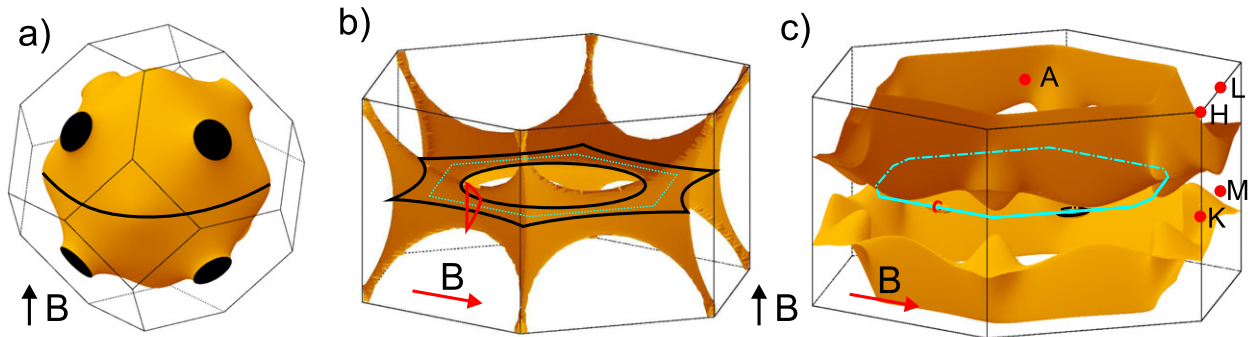


Figure 22. Fermi surfaces for Cu (a) and Mg (b) with extremal orbits for different directions of the applied magnetic field. For TI (c) a constant energy surface slightly above the Fermi energy ($E_F + 0.02$ Ryd) was chosen to create extremal orbits enclosing a line of contact points. These orbits on tiny ellipsoids in the Γ M direction are shown in red and black for \mathbf{B} fields parallel and perpendicular to the hcp base plane respectively. The lines of degeneracy are shown as blue dashed lines.

is independent of the actual form of the loop. The effect is topological since only whether the line penetrates the orbit or not is relevant. This result dramatically affects the analysis of de Haas-van Alphen experiments since the quantization condition of equation (103) will be either

$$S(E_\nu, k_z) = 2\pi\hbar e B_z \nu \quad (106)$$

or

$$S(E_\nu, k_z) = 2\pi\hbar e B_z (\nu + \frac{1}{2}) \quad (107)$$

depending on whether the orbit encloses a line of degeneracies or not, respectively.

Clearly, what happens to such lines of degeneracies in the presence of spin and spin-orbit coupling is an interesting and fundamental question, since in that case the bands are formed from states that are Kramers doublets and two such doublets are infinitely unlikely to be degenerate. In the limit of small spin-orbit coupling this question was investigated by Mikitik and Sharlai [62]. They found that the Berry phase contribution becomes zero, but for nonmagnetic inversion symmetric systems there is a contribution to the area enclosed by a Landau orbit arising from the magnetization

part of equation (105). However, the case of strong spin-orbit coupling remains an open problem.

5. Conclusion

In the presence of a periodic crystal potential the free electron spectrum $\mathcal{E}_{\mathbf{k}} = \frac{\hbar^2 k^2}{2m}$ breaks up into bands with nontrivial dispersion relations $\mathcal{E}_{n\mathbf{k}}$. It turns out that the adiabatic dynamics of wave packets, constructed by superposition of all \mathbf{k} states but a limited number of bands n , features a Berry connection $\mathbf{A}_n(\mathbf{k})$ and a corresponding curvature $\Omega_n(\mathbf{k})$, which account for the influence of the neglected bands [6, 7]. Moreover, these geometrical properties of the band structure play an essential role in describing a number of important physical phenomena such as spin and charge transport, electric polarization and orbital magnetization [1]. What makes these remarkable developments particularly interesting from the point of view of *first-principle* electronic structure calculations is the fact that the curvature $\Omega_n(\mathbf{k})$ is a very rapidly varying function of \mathbf{k} and it depends on intricate details of the band structure. Consequently, devising methods for computing $\Omega_n(\mathbf{k})$ have recently become a very active

field of research. In this paper we sketched three approaches to the problem: one is based on multiple scattering theory (KKR, similarly LMTO), another one on the Wannier function representation of *first-principle* bands and the third one on direct evaluation of a Kubo-like formula. We pointed out the differences and highlighted the similarities in the way the derivatives with respect to the wave vector \mathbf{k} enter the problem. We stressed the importance of level crossings which give rise to curvatures $\Omega_n(\mathbf{k})$ whose \mathbf{k} dependence is that of the Dirac monopole and the more exotic avoided crossings of Kramers degenerate bands whose curvature is a non-Abelian gauge field. As illustrations of results by the various methods, we presented calculations of the intrinsic contribution to the anomalous and spin Hall conductivity and the Berry curvature for a variety of systems as well as the manifestation of the Berry phase in de Haas–van Alphen oscillations.

In that review we concentrated on the Berry curvature caused by the parameter \mathbf{k} in the Hamiltonian for Bloch electrons. However, from the general point of view any slowly changing parameter in a Hamiltonian causes curvatures which might be of interest in future considerations. From that perspective, curvatures associated with spatial or temporal parameters will represent new computational challenges.

Very recently, after finalizing this manuscript, another method calculating the Berry curvature was published [64]. It is based on a finite-differences approach within the augmented spherical wave scheme. The method was originally developed for calculating directly the Z_2 invariants of topological insulators and not for expressing the Berry curvature \mathbf{k} -point by \mathbf{k} -point [65, 66]. This is the reason why we missed it. We would like to thank Professor Jürgen Kübler for discussing this new method with us.

Acknowledgments

One of us (BLG) would like to thank Professor Michael Berry for many fruitful conversations on the topic of this article. MG acknowledges support from the German Research Foundation (DFG) via a Research Fellowship (GR 3838/1-1). In addition, this work was supported by the DFG via SFB 762.

References

- [1] Xiao D, Chang M-C and Niu Q 2010 Berry phase effects on electronic properties *Rev. Mod. Phys.* **82** 1959
- [2] Marder M P 2000 *Condensed Matter Physics* (New York: Wiley)
- [3] Berry M V 1984 Quantal phase factors accompanying adiabatic changes *Proc. R. Soc. A* **392** 45
- [4] Culcer D, Yao Y and Niu Q 2005 Coherent wave-packet evolution in coupled bands *Phys. Rev. B* **72** 085110
- [5] Shindou R and Imura K-I 2005 Noncommutative geometry and non-Abelian Berry phase in the wave-packet dynamics of Bloch electrons *Nucl. Phys. B* **720** 399–435
- [6] Wilczek F and Zee A 1984 Appearance of gauge structure in simple dynamical systems *Phys. Rev. Lett.* **52** 2111
- [7] Sundaram G and Niu Q 1999 Wave-packet dynamics in slowly perturbed crystals: gradient corrections and Berry-phase effects *Phys. Rev. B* **59** 14915
- [8] Kramers H A 1930 General theory of paramagnetic rotation in crystals *Proc. R. Acad. Sci. Amsterdam* **33** 959
- [9] Elliott R J 1954 Theory of the effect of spin–orbit coupling on magnetic resonance in some semiconductors *Phys. Rev.* **96** 266
- [10] Berry M V and Wilkinson M 1984 Diabolical points in the spectra of triangles *Proc. R. Soc. A* **392** 15
- [11] Pientka F 2010 Geometrical concepts in the band theory of solids *Diploma Thesis* University Halle-Wittenberg <http://www.physik.uni-halle.de/theorie/ag/qtfk/mitarbeiter/pientka/>
- [12] Hals K M D, Nguyen A K, Waintal X and Brataas A 2010 Effective magnetic monopoles and universal conductance fluctuations *Phys. Rev. Lett.* **105** 207204
- [13] Dirac P A M 1948 The theory of magnetic poles *Phys. Rev.* **74** 817
- [14] Thouless D J, Kohmoto M, Nightingale M P and den Nijs M 1982 Quantized Hall conductance in a two-dimensional periodic potential *Phys. Rev. Lett.* **49** 405
- [15] Simon B 1983 Holonomy, the quantum adiabatic theorem, and Berry’s phase *Phys. Rev. Lett.* **51** 2167
- [16] Haldane F D M 2004 Berry curvature on the Fermi surface: anomalous Hall effect as a topological Fermi-liquid property *Phys. Rev. Lett.* **93** 206602
- [17] von Neumann J and Wigner E 1929 Über das Verhalten von eigenwerten bei adiabatischen prozessen *Phys. Z.* **30** 467
- [18] Bohm A, Mostafazadeh A, Koizumi H, Niu Q and Zwanziger J 2003 *The Geometric Phase in Quantum Systems* (Berlin: Springer)
- [19] Gradhand M, Fedorov D V, Pientka F, Zahn P, Mertig I and Györfy B L 2011 On calculating the Berry curvature of Bloch electrons using the KKR method *Phys. Rev. B* **84** 075113
- [20] Fabian J and Das Sarma S 1998 Spin relaxation of conduction electrons in polyvalent metals: theory and a realistic calculation *Phys. Rev. Lett.* **81** 5624
- [21] Wang X, Yates J R, Souza I and Vanderbilt D 2006 *Ab initio* calculation of the anomalous Hall conductivity by Wannier interpolation *Phys. Rev. B* **74** 195118
- [22] Gradhand M, Czerner M, Fedorov D V, Zahn P, Yavorsky B Yu, Szunyogh L and Mertig I 2009 Spin polarization on Fermi surfaces of metals by the KKR method *Phys. Rev. B* **80** 224413
- [23] Pientka F, Gradhand M, Fedorov D V, Mertig I and Györfy B L 2012 Gauge freedom for degenerate Bloch states *Phys. Rev. B* submitted
- [24] Zeller R, Dederichs P H, Újfalussy B, Szunyogh L and Weinberger P 1995 Theory and convergence properties of the screened Korringa–Kohn–Rostoker method *Phys. Rev. B* **52** 8807
- [25] Szunyogh L, Újfalussy B, Weinberger P and Kollár J 1994 Self-consistent localized KKR scheme for surfaces and interfaces *Phys. Rev. B* **49** 2721
- [26] Strange P 1998 *Relativistic Quantum Mechanics with Applications in Condensed Matter and Atomic Physics* (Cambridge: Cambridge University Press)
- [27] Slater J C and Koster G F 1954 Simplified LCAO method for the periodic potential problem *Phys. Rev.* **94** 1498
- [28] Jones M D and Albers R C 2009 Spin–orbit coupling in an f-electron tight-binding model: electronic properties of Th, U, and Pu *Phys. Rev. B* **79** 045107
- [29] Marzari N, Souza I and Vanderbilt D 2003 An introduction to maximally-localized wannier functions *Psi-k Newsletter* **57** 129 (Scientific Highlight of the Month) http://www.psi-k.org/newsletters/News_57/Highlight_57.pdf
- [30] Marzari N and Vanderbilt D 1997 Maximally localized generalized Wannier functions for composite energy bands *Phys. Rev. B* **56** 12847
- [31] Wang X, Vanderbilt D, Yates J R and Souza I 2007 Fermi-surface calculation of the anomalous Hall conductivity *Phys. Rev. B* **76** 195109

- [32] Roman E, Mokrousov Y and Souza I 2009 Orientation dependence of the intrinsic anomalous Hall effect in hcp Cobalt *Phys. Rev. Lett.* **103** 097203
- [33] Kubo R 1957 Statistical-mechanical theory of irreversible processes *J. Phys. Soc. Japan* **12** 570
- [34] Karplus R and Luttinger J M 1954 Hall effect in ferromagnetics *Phys. Rev.* **95** 1154
- [35] Sinova J, Jungwirth T, Kucera J and MacDonald A H 2003 Infrared magneto-optical properties of (III,Mn)V ferromagnetic semiconductors *Phys. Rev. B* **67** 235203
- [36] Fang Z, Nagaosa N, Takahashi K S, Asamitsu A, Mathieu R, Ogasawara T, Yamada H, Kawasaki M, Tokura Y and Terakura K 2003 The anomalous Hall effect and magnetic monopoles in momentum space *Science* **302** 92
- [37] Guo G Y, Yao Y and Niu Q 2005 *Ab initio* calculation of the intrinsic spin Hall effect in semiconductors *Phys. Rev. Lett.* **94** 226601
- [38] Yao Y and Fang Z 2005 Sign changes of intrinsic spin Hall effect in semiconductors and simple metals: first-principles calculations *Phys. Rev. Lett.* **95** 156601
- [39] Wang C S and Callaway J 1974 Band structure of nickel: spin-orbit coupling, the Fermi surface, and the optical conductivity *Phys. Rev. B* **9** 4897
- [40] Guo G Y and Ebert H 1995 Band-theoretical investigation of the magneto-optical Kerr effect in Fe and Co multilayers *Phys. Rev. B* **51** 12633
- [41] Yao Y, Kleinman L, MacDonald A H, Sinova J, Jungwirth T, Wang D, Wang E and Niu Q 2004 First principles calculation of anomalous hall conductivity in ferromagnetic bcc Fe *Phys. Rev. Lett.* **92** 037204
- [42] Culcer D, Sinova J, Sinitsyn N A, Jungwirth T, MacDonald A H and Niu Q 2004 Semiclassical spin transport in spin-orbit-coupled bands *Phys. Rev. Lett.* **93** 046602
- [43] Sinova J, Culcer D, Niu Q, Sinitsyn N A, Jungwirth T and MacDonald A H 2004 Universal intrinsic spin Hall effect *Phys. Rev. Lett.* **92** 126603
- [44] Vernes A, Györfy B L and Weinberger P 2007 Spin currents, spin-transfer torque, and spin-Hall effects in relativistic quantum mechanics *Phys. Rev. B* **76** 012408
- [45] Lowitzer S, Gradhand M, Ködderitzsch D, Fedorov D V, Mertig I and Ebert H 2011 Extrinsic and intrinsic contributions to the spin Hall effect of alloys *Phys. Rev. Lett.* **106** 056601
- [46] Solovyyev I V 2003 Effects of crystal structure and on-site Coulomb interactions on the electronic and magnetic structure of $A_2Mo_2O_7$ ($A = Y, Gd, \text{ and } Nd$) pyrochlores *Phys. Rev. B* **67** 174406
- [47] Guo G Y, Murakami S, Chen T-W and Nagaosa N 2008 Intrinsic spin Hall effect in platinum: first-principles calculations *Phys. Rev. Lett.* **100** 096401
- [48] Guo G Y 2009 *Ab initio* calculation of intrinsic spin Hall conductivity of Pd and Au *J. Appl. Phys.* **105** 07C701
- [49] Freimuth F, Blügel S and Mokrousov Y 2010 Anisotropic spin Hall effect from first principles *Phys. Rev. Lett.* **105** 246602
- [50] Seemann K M, Mokrousov Y, Aziz A, Miguel J, Kronast F, Kuch W, Blamire M G, Hindmarch A T, Hickey B J, Souza I and Marrows C H 2010 Spin-orbit strength driven crossover between intrinsic and extrinsic mechanisms of the anomalous Hall effect in the epitaxial $L1_0$ -ordered ferromagnets FePd and FePt *Phys. Rev. Lett.* **104** 076402
- [51] Zhang H, Blügel S and Mokrousov Y 2011 Anisotropic intrinsic anomalous Hall effect in ordered 3dPt alloys *Phys. Rev. B* **84** 024401
- [52] Zhang H, Freimuth F, Blügel S and Mokrousov Y 2011 Role of spin-flip transitions in the anomalous Hall effect of FePt alloy *Phys. Rev. Lett.* **106** 117202
- [53] Weischenberg J, Freimuth F, Sinova J, Blügel S and Mokrousov Y 2011 *Ab initio* theory of the scattering-independent anomalous Hall effect *Phys. Rev. Lett.* **107** 106601
- [54] Kovalev A A, Sinova J and Tserkovnyak Y 2010 Anomalous Hall effect in disordered multiband metals *Phys. Rev. Lett.* **105** 036601
- [55] Xiao D, Yao Y, Fang Z and Niu Q 2006 Berry-phase effect in anomalous thermoelectric transport *Phys. Rev. Lett.* **97** 026603
- [56] Mikitik G P and Sharlai Yu V 1998 Semiclassical energy levels of electrons in metals with band degeneracy lines *J. Exp. Theor. Phys.* **87** 747
- [57] Mikitik G P and Sharlai Yu V 1999 Manifestation of Berry's phase in metal physics *Phys. Rev. Lett.* **82** 2147
- [58] Mikitik G P and Sharlai Yu V 2004 Berry phase and de Haas-van Alphen effect in $LaRhIn_5$ *Phys. Rev. Lett.* **93** 106403
- [59] Mikitik G P and Sharlai Yu V 2007 The phase of the Haas-van Alphen oscillations, the Berry phase, and band-contact lines in metals *Low Temp. Phys.* **33** 439
- [60] Gosselin P, Boumrar H and Mohrbach H 2008 Semiclassical quantization of electrons in magnetic fields: the generalized Peierls substitution *Europhys. Lett.* **84** 50002
- [61] Roth L M 1966 Semiclassical theory of magnetic energy levels and magnetic susceptibility of Bloch electrons *Phys. Rev.* **145** 434
- [62] Mikitik G P and Sharlai Yu V 2002 g factor of conduction electrons in the de Haas-van Alphen effect *Phys. Rev. B* **65** 184426
- [63] Erikson O, Ohlsen H and Calais J L 1989 Conduction-electron Zeeman splitting in the noble metals *Phys. Rev. B* **40** 5961
- [64] Kübler J and Felser C 2012 Berry curvature and the anomalous Hall effect in Heusler compounds *Phys. Rev. B* **85** 012405
- [65] Xiao D, Yao Y, Feng W, Wen J, Zhu W, Chen X, Stocks G M and Zhang Z 2010 Half-Heusler compounds as a new class of three-dimensional topological insulators *Phys. Rev. Lett.* **105** 096404
- [66] Fukui T and Hatsugai Y 2007 Quantum spin Hall effect in three dimensional materials: lattice computation of Z_2 topological invariants and its application to Bi and Sb *J. Phys. Soc. Jap.* **76** 053702